國立交通大學

電子物理研究所

碩士論文

掃描式電場力顯微術於氮化鎵島狀結構之研究

Studies of GaN Islands by Scanning Electric Force Microscopy

研 究 生：黃鐘逸

指導教授：陳衛國 教授

中華民國九十四年七月

掃描式電場力顯微術於氮化鎵島狀結構之研究

Studies of GaN Islands by Scanning Electric Force Microscopy

研 究 生：黃鐘逸　　Student： Chung-I Huang

指導教授： 陳衛國 教授　　Advisor： Prof. Wei-Kuo Chen

國立交通大學

電子物理研究所

碩士論文

A Thesis
Submitted to Institute of Electrophysics
College of Science
National Chiao Tung University
in Partial Fulfillment of the Requirements
for The Degree of Master of Physics
in
Electrophysics
July 2005
Hsinchu, Taiwan, Republic of China

中華民國九十四年七月

Acknowledgment

『當機會從我們眼前晃過去時，這時…我們就該把釣竿和誘餌準備好…

再用耐心當水泥，把機會建築的更佳堅固，

堅持到最後一秒鐘。』

摘自「這一生都是你的機會」 Alex Rovira 著

因為堅持，我熬過了最艱難的時期，挺到了要動筆寫致謝的此時，這代表著論文的完成與碩士班生涯的即將結束，內心除了無法形容的欣喜外，卻也滿懷感激。

能順利在兩年內完成論文與口試，首先得謝謝指導教授陳衛國老師願意給我機會，由於陳老師不厭其煩的諄諄教誨，使我在做研究方面，和待人處事上都有所精進，此外，李明知老師、周武清老師、陳文雄老師也都在我論文研究過程中，適時給予關鍵的指導與鼓勵。更感謝姜崇義博士、林文仁博士在口試時的建議，讓這份論文研究能更臻完善！

實驗室伙伴們的幫忙與生活上的照應也讓我很窩心！感謝李寧、張富欽、古慶順、柯文政、陳京玉、傅振邦、蔡佼哲、顏國錫、何志偉等學長（嫂）的指導與照顧，特別是李寧學長，總是在我實驗遭遇困難時，放下手邊工作與我討論，從而度過重重難關。更要謝謝同學逸文、信志、碧軒、承勳、佳進在這一段日子以來的陪伴與鼓勵，還有學弟妹士凱、啟仁、維偲、泰鑫、士傑、家禎、尚樺，以及其他許許多多的朋友，由於你們，讓這段日子有了不少值得留戀的回憶。

最後，也是最重要的，是我的父母與家人，因為你們的支持，使我得以專心完成學業，謝謝你們！

……這兩年的點、點、滴、滴……

我想，

就隨著這篇致謝的署名，

讓它

寫下句號吧。

鐘逸　　於新竹交大

Index

Acknowledgment

Abstract (Chinese Version)……………………………………………………ii

Abstract (English Version)………………………………………………..... iv

Chapter 1. Introduction………………………………………………......1

Chapter 2. Theoretical Backgrounds....……………………………………...5

2.1 Atomic Force Microscopy (AFM)………………………………..5

2.2 Scanning Electric Force Microscopy (EFM)……………………..9

2.3 Scanning Kelvin Probe Microscopy (SKM)…….……………….17

Chapter 3. Experiments……………………………………………………18

3.1 Sample Preparation…………………………………………….18

3.2 Experiment Procedure……………………………………………...21

3.3 Analysis Instruments………………………………………………24

Chapter 4. Results and Discussion………………...………………………26

4.1 Model………………………………………………………….26

4.2 Calibration of Work Function of Tip…………………………….29

4.3 ω-$F_{ESC\text{-}tip}$ from Plane on Sample……………………..…………..35

4.4 Morphology and Force Mapping of GaN Island………………...41

4.5 ω-$F_{ESC\text{-}tip}$ from the Single GaN Island...……………………...….47

Chapter 5. Conclusion…..……..……………………………………………..65

Appendix…………………………………………………………………67

Reference…………………………………………………………………68

掃描式電場力顯微術於氮化鎵島狀結構之研究

研究生：黃鐘逸　　　　　　　　　　　　指導教授：陳衛國　博士

國立交通大學

電子物理研究所

中文摘要

在本論文中，經由掃描式電場力顯微術（EFM）的原理，我們發展出一個模型。利用這個模型，我們可以求出所使用的原子力顯微術探針的表面功函數絕對值，並在不同探針與樣品間距，量測以基頻頻率 ω 和 2 倍頻率 2ω 振盪的受力（分別以 F_{ω} 和 $F_{2\omega}$ 表示）的映像來計算探針與樣品表面靜電荷之間的庫侖力。經過測定功函數後的探針可以用來量測其他樣品的表面功函數。EFM 的實驗結果顯示，在圓盤狀氮化鎵島狀結構的樣品上，F_{ω} 和 $F_{2\omega}$ 的映象同樣具有很好的解析表面結構的能力，我們還發現島狀結構區域的 F_{ω} 和 $F_{2\omega}$ 受力強度較平坦處小，而且島狀結構高度愈高，受力愈小。我們也分別計算在矽晶圓與氮化鎵島狀結構表面上的靜電荷與探針之間以 ω 頻率振盪的庫侖力大小，發現其作用模式在矽晶圓上較適合用圓錐體模型

來解釋，在氮化鎵島狀結構上的實驗結果用點電荷對圓盤的模型來解釋較佳，我們將這兩種差異歸因於樣品表面靜電荷的區域相對於探針的尺寸大小所造成的電場分佈不一樣所致。在無窮大平板（如本實驗的矽晶圓）上，表面靜電荷所生成的電場是均勻分佈的，作用在探針上是影響探針整體，所以可用圓錐體模型來解釋實驗結果。但在圓盤狀氮化鎵島狀結構上的靜電荷所生成的電場並不均勻且隨高度增加其強度會快速減少，在計算探針與氮化鎵島狀結構上的靜電荷之間以 ω 頻率振盪的庫侖力時，探針尖端的球體是主要的受力位置，所以可以用點電荷對圓盤的模型來解釋其實驗結果。

Studies of GaN Islands by Scanning Electric Force Microscopy

Student: Chung-I Huang **Advisor: Dr. Wei-Kuo Chen**

Institute of Electrophysics

National Chiao-Tung University

Abstract

We had developed a model based on the equations related to the principle of scanning electric force microscopy (EFM). By this model, we can obtain the surface work function of the tip we used in our atomic force microscopy (AFM) system and calculate the ω-term Coulombic force between the tip and the surface electrostatic charge (ESC) on the sample in the ω-term and 2ω-term force (signed F_{ω} and $F_{2\omega}$, respectively) mappings at different tip-sample distances. The calibrated value of tip work function can be used to characterize the surface work function of other samples. The EFM results show that the F_{ω} and $F_{2\omega}$ force mappings on disk-like GaN islands can be well-resolved. The intensities of the electric forces F_{ω} and $F_{2\omega}$ on the region of GaN islands are comparatively lower as respect to that of the plane surface. The higher the island

is, the lower the value of intensity is. We can also calculate the ω-term Coulombic force between the tip and the surface ESC on Si wafer and that on the disk-like GaN island, respectively. We found that the reactive Coulombic force can be interpreted by the cone model on the Si wafer, and by the charged point-disk model on the disk-like GaN island, respectively. We believed that such discrepancy can be attributed to the difference of electric field distribution resulted from the dimension of the ESC distribution region on the sample surface as compared with the tip. The uniform electric field acting on all part of the tip above the infinite plane (such as the Si wafer) results in using the cone mode to interpret the experimental results. But, in the single disk-like GsN island whose electric field resulted from ESC on surface is not uniform and decreases rapidly with increasing height. The sphere of the tip is the main position suffered the ω-term Coulombic force between the tip and the surface ESC on the single disk-like GaN island. As a result, we can use the charged point-disk model to interpret the ω-term Coulombic force between the tip and the ESC purely on the single disk-like GaN island.

Chapter 1 Introduction

In recent years, scanning Kelvin probe microscopy (SKM) has become an important characterization technique for semiconductors. [1-13] Utilizing SKM technique we can probe the contact potential difference (CPD) which represents the difference of work function between metal tip and sample surface regarding to the micro-structure on the semiconductor materials [14-16] or devices [3-13].

According to the report of G. Koley *et al.* [17], the CPD voltage (V_{CPD}) is increased as the tip-sample distance is increased, as shown in Fig. 1.1. In other words, the V_{CPD} is dependent on the distance between tip and sample surface. The equation of the associated electrostatic ω-term force can be expressed as [17-22]

$$F_{\omega} = -\frac{\partial C}{\partial Z}(V_{dc} - V_{CPD})V_{ac} + \frac{Q_t Q_s}{4\pi\varepsilon_0 Z^2} \quad (1\text{-}1)$$

where Q_t is the charge on the tip surface, Q_s is the charge on the sample surface, V_{CPD} is the difference between the work functions of the sample surface and the probe tip surface, C is the capacitance between tip and sample, Z is the tip to sample distance, and ε_0 is the dielectric constant of the medium between tip and sample. It is noted that we use point-charge to point-charge model to describe the actual situation of atomic force microscopy (AFM) tip and sample for simplicity. [23] There is also other report, J. W. Hong *et al.*, for example [24-31],

which describe the charge on the sample surface as a uniform charge density signed as σ_b and the second term of Eq. (1.1) is rewrote as $\frac{Q_t \sigma_b}{2\varepsilon_0}$ for infinite charged plane sample. Here we use the form of Eq. (1-1) (point-charge to point-charge model) to interpret Fig. 1.1, which are both quoted from Ref. 17, to debate continuously in this chapter to maintain the consistence. In order to measure the SKM V_{dc} signal, a feedback loop is used to adjust the external biasd voltage V_{dc} between the tip and the sample such that the vibration amplitude of the ω-term force F_ω vanishes. In Fig. 1.1, we find the voltage (so-called "SKM resulted signal V_{dc}") varies strongly at smaller distance, and tends to saturation as the distance beyond 1.5μm. It can be seen more clearly in Eq. (1-1). When the tip-sample distance is smaller than 1μm, the SKM resulted signal V_{dc} is smaller, and its value is affected strongly by the second term in a short distance, as shown in Fig. 1.1. And the second term in Eq. (1-1) can be ignored when Z is larger than about 2μm. That is to say that the V_{dc} is equal to V_{CPD} under such a situation. In short, we can obtain the exact value of V_{CPD} when Z is large but low spatial resolution. On the other hand, when Z is always small, high spatial resolution can be obtained and precise V_{CPD} can not be retrieved.

From the above discussions, it is learned that obtaining the V_{CPD} value at nano-scale remains a challenge. We must examine the second term of Eq. (1-1) more thoroughly. So far, G. Koley *et al.* has viewed the second tern in Eq. (1-1), Coulombic force, acting on the tip in SKM measurement as the point-point

model [17-22], parallel-plate capacitance model [24-25] or point-plane model [26-31] to characterize the surface properties. But these models are too simple to correspond to the real condition and nobody has studied the characteristic of the Coulombic force between the tip and the surface charge on the sample. In this study, we set up a series of experiments to measure the Coulombic force acting on the tip on different sample surface (plane and disk-shape island) and find a model for explaining the tip-sample distance dependence of the Coulombic force at fundamental frequency.

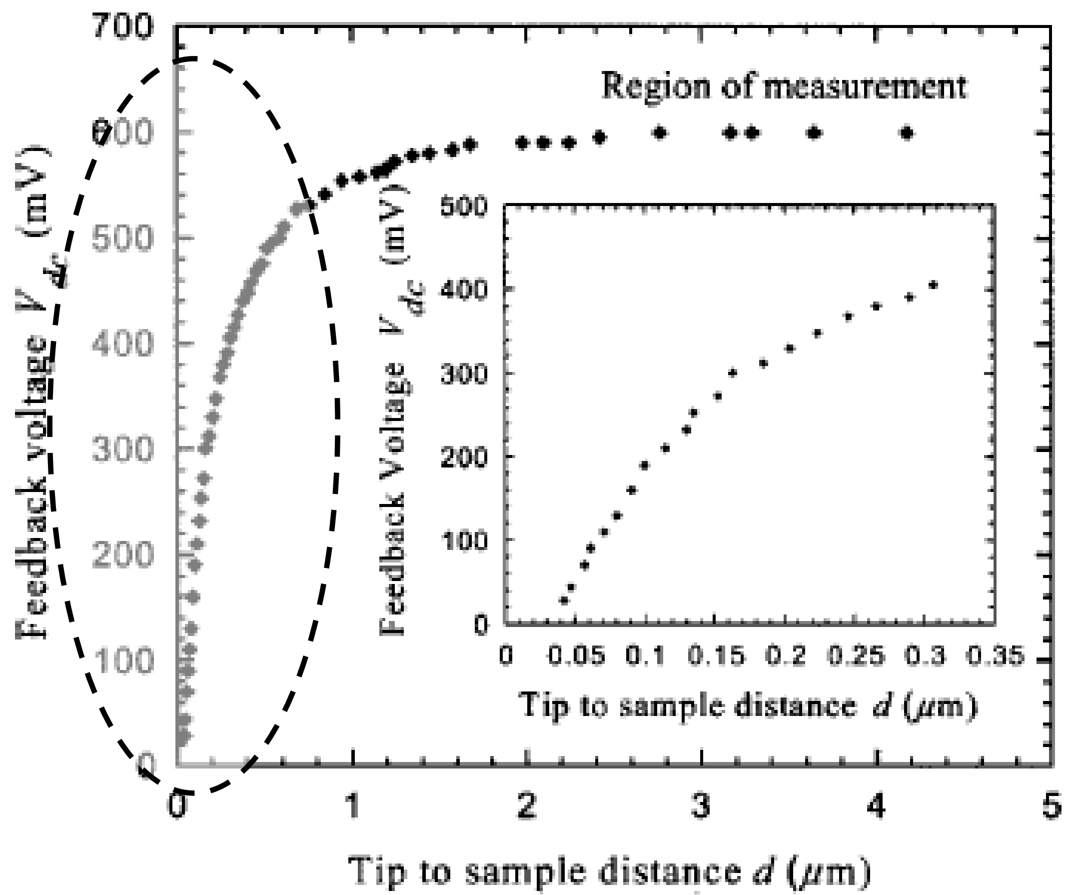

Fig. 1.1. The SKM feedback voltage is dependent on the tip to sample distance. [17]

Chapter 2 Theoretical Backgrounds

In this chapter, we describe the measuremental principle of atomic force microscopy (AFM), scanning electric force microscopy (EFM), and scanning Kelvin probe microscopy (SKM).

2.1 Atomic Force Microscopy (AFM)

The basic operational principle of AFM is to bias the cantilever with an AC and a DC voltages. When the AC signal was tuned to the resonance frequency of the cantilever, the cantilever will vibrate with a maximum amplitude. After placing the probe on the holder, we can move the probe with tip on the cantilever to the sample surface. When the tip is put closer to the sample, the attractive and repulsive forces will affect the displacement amplitude of the cantilever. Utilizing the reflective optical signals from the cantilever, we may analyze the surface properties of the sample. Generally, there are three modes to obtain the sample morphology in the AFM system.

We introduce these modes as follows, with the diagram shown in Fig. 2.1.1.

(I) Contact Mode

In this mode, the cantilever touches the surface and scans over the sample surface. Via the electrical feedback loop, the piezoelectric scanner enforces the cantilever with a constant force. As the surface height changes, the system will

detect the deflection signals of the cantilever and then it modulates the scanner's height to keep the force at a constant value. The modulation of the scanner's height will be recorded and processed by the controller and the software, which provides us the information of the sample's morphology property.

(II) Non-Contact Mode

In order to avoid the destruction of the probe in scanning, we operate AFM system in non-contact mode. Utilizing the long range Van der Waal's force between the tip and sample surface it vibrates with a smaller amplitude. But the long range force is not sensitive to the changes of the height, it needs advanced modulation technology to enhance the signal to noise ratio. In the ambient environment, the non-contact mode's resolution is only about 50nm. If we want to obtain the better images, the system must be loaded into the vacuum chambers.

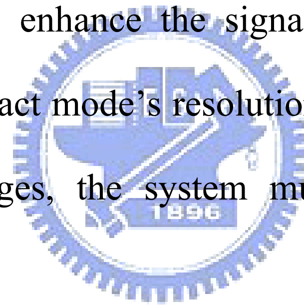

(III) Semi-Contact Mode

The semi-contact mode (or named tapping mode) is modified from the non-contact mode, the amplitude of the cantilever is enlarged, and the height between the tip and the sample is reduced. Through the modulation technology, the changes of the cantilever's amplitude affected by the surface height are recorded, and one obtains the morphology through the software analysis. The tapping mode is also more sensitive to interact with sample surface, and we may obtain the AFM image at higher resolution as compared with the non-contact mode. This mode is also applicable to characterize the surface distribution of the

magnetic and electric field, elasticity and viscosity.

Besides the morphology measurements, the AFM system can also be utilized for other researches, such as the micro I-V measurements, spreading resistance distribution, and the nano-lithography. All the new functions are still under developing. [23]

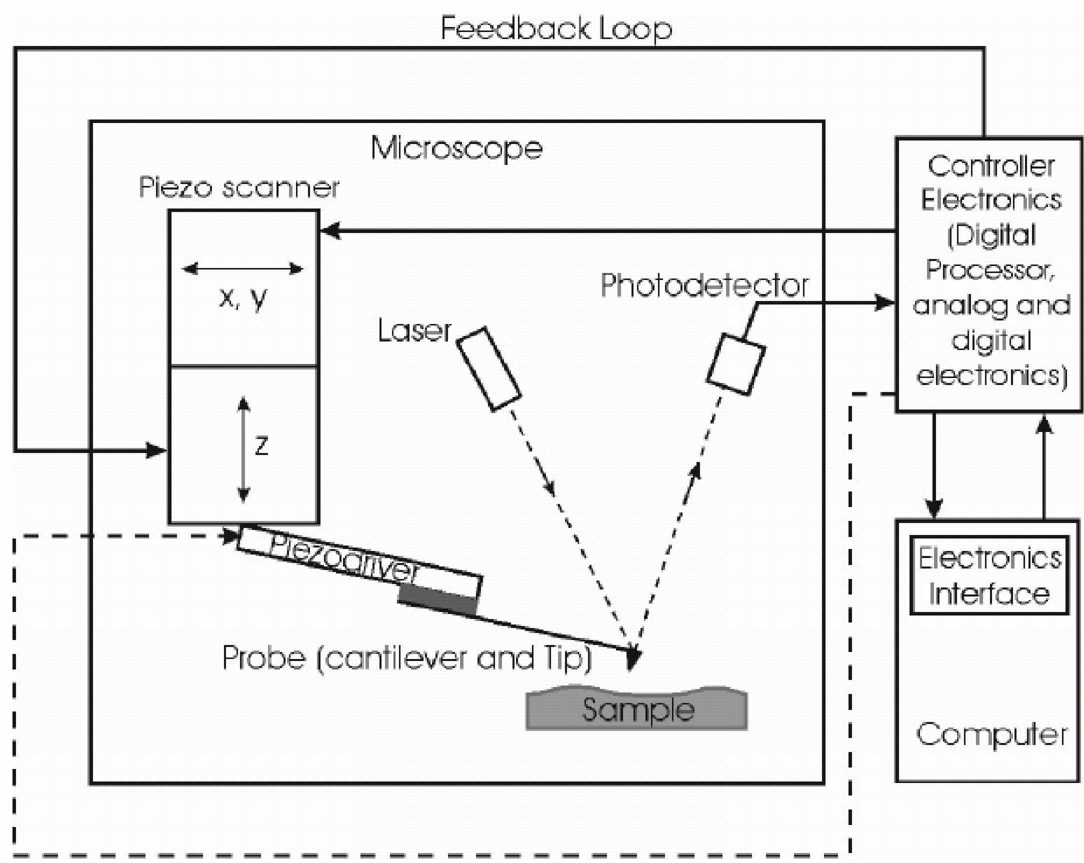

Fig. 2.1.1. Schematic diagram of AFM system. (from NT-MDT Manual)

2.2 Scanning Electric Force Microscopy (EFM)

The scanning electrical force microscopy (EFM) is semi-contact AFM technique, which uses a metal-coated tip to probe electrical properties of surface under AC operation. In our studies, we used Pt-coated tip. The schematic diagram of scanning EFM is shown in Fig. 2.2.1.

The scanning EFM mapping is obtained by two-pass method. The corresponding schematic diagram is shown in Fig. 2.2.2. In the semi-contact mode scanning, the first pass is used to measure the sample surface morphology. Then, at the second pass, the probe is withdrawn from (or approached to) the sample surface relative to the first pass with a distance ΔZ and passed at this height over the sample surface to probe other local signals corresponding to the morphology image, such as the intensity of the electrostatic force acting on the tip in this studies. But the second-pass scanning process may be with different scanning parameters. In scanning EFM, we apply an AC and a DC voltage (V_{ac} and V_{dc} , respectively) between the tip and sample, as shown in Fig. 2.2.3. At the same time, the scanning EFM system monitors the cantilever vibration due to the electrostatic force at the fundamental frequency ω and second harmonic frequency 2ω of the applied V_{ac}. Via the reflected light from vibrating cantilever being detected by the photodiode of the scanning EFM system without feedback (Fig. 2.2.1), the magnitude of force acting on tip is transferred to a current signal. In the continuous chapters, all of the force magnitude is expressed by current.

In the scanning probe microscopy (SPM) system, the structure between the

metal tip and the sample can be regarded as a capacitance. When we bias the applied voltage on the tip, the induced charge would appear on the tip surface and the sample surface. Besides, there is also some local surface electrostatic charge (ESC) on the sample surface which may come from the broken bonds, micro structures, and interface, etc., as shown in Fig. 2.2.4. The ESC already exists under thermal equilibrium and the opposite pole of charge exists in the opposite side of the space charge region of the semiconductor sample to maintain charge neutrality. In our study, the applied voltage is maintained under 1 volt for DC voltage and 0.1 volt for AC voltage. We assume that the applied voltage would not change the distribution of surface ESC.

If we applied a voltage $V_{applied,tip} = V_{dc} + V_{ac}\sin\omega t$ between the tip and the sample, the total voltage between them is U as written below.

$$U = \left(V_{dc} - V_{CPD}\right) + V_{ac}\sin\omega t \quad (2\text{-}1)$$

The electrostatic force acting on the tip is

$$F = -\frac{\partial E}{\partial Z} = -\frac{U^2}{2}\frac{\partial C}{\partial Z} \quad (2\text{-}2)$$

where E is the electrostatic energy, C is the capacitance between the tip and the sample, and Z is the distance between the tip and the sample. If there is local surface ESC on the sample surface and we assume that the ESC is uniform distribution on the surface. The electrostatic force includes two components: capacitive component and Coulombic component. Thus, Eq. (2-2) is rewrote as

$$F=-\frac{U^2}{2}\frac{\partial C}{\partial Z}+F_{ESC-tip} \tag{2-3}$$

where $F_{ESC\text{-}tip}$ is the Coulombic force acting on the tip from the surface ESC on the sample. By Substituting U by Eq. (2-1), we find that F consists of three parts at dc, ω, and 2ω:

$$\begin{aligned}F&=-\frac{1}{2}\frac{\partial C}{\partial Z}\left[\left(V_{dc}-V_{CPD}\right)+V_{ac}\sin\omega t\right]^2+F_{ESC-tip}\\&=-\frac{1}{2}\frac{\partial C}{\partial Z}\Big[\left(V_{dc}-V_{CPD}\right)^2+2\left(V_{ac}-V_{CPD}\right)V_{ac}\sin\omega t\\&\quad+V_{ac}{}^2\sin^2\omega t\Big]+F_{ESC-tip}(dc,\omega)\\&=-\frac{1}{2}\frac{\partial C}{\partial Z}\Big[\left(V_{dc}-V_{CPD}\right)^2+2\left(V_{ac}-V_{CPD}\right)V_{ac}\sin\omega t\\&\quad+V_{ac}{}^2\frac{1-\cos 2\omega t}{2}\Big]+F_{ESC-tip}(dc,\omega)\\&=F_{dc}+F_{\omega}\sin\omega t+F_{2\omega}\cos 2\omega t\end{aligned}$$

where

$$F_{dc}=-\frac{1}{2}\frac{\partial C}{\partial Z}(V_{dc}-V_{CPD})^2+F_{ESC-tip,dc}$$

$$F_{\omega}=-\frac{\partial C}{\partial Z}(V_{dc}-V_{CPD})V_{ac}+F_{ESC-tip,\omega} \tag{2-4}$$

$$F_{2\omega}=\frac{1}{4}\frac{\partial C}{\partial Z}V_{ac}^2 \tag{2-5}$$

F_{dc}, the ω-force F_{ω}, and the 2ω-force $F_{2\omega}$ can be measured separately using lock-in amplifiers without feedback, as shown in Fig. 2.2.1. The ω-force acting on the tip consists of two kinds of interaction. One is the tip and the sample

surface induced charge (capacitive component, first term in Eq. (2-4)), and the other is the tip and the surface ESC (Coulombic component, second term in Eq. (2-4)), as shown in Fig. 2.2.4. The second interaction plays an important role in determining SKM and scanning EFM signals. We would discuss in detail in this studies.

It is noted that the F_{dc} and the ω-force F_{ω} have the term $F_{ESC\text{-}tip}$, but the 2ω-force $F_{2\omega}$ does not. The reason can be explained as follows. For simplicity, we regard the situation as the plate capacitance model and assume that there are point charges Q_s and Q_e on the sample surface. Q_e is induced charge resulted from the applied voltage, Q_s is ESC on the sample surface, and Q_t is the charge on the metal tip, as shown in Fig. 2.2.5. We can write the following equation.

$$Q_e = CV = C(V_{dc} + V_{ac}\sin\omega t)$$

The Q_t includes $-Q_e$ and the image charge of Q_s, as written in the following

$$Q_t = -(Q_s + Q_e) = -(Q_s + CV_{dc} + CV_{ac}\sin\omega t)\cdot$$

According to Coulomb's law, $F_{ESC\text{-}tip}$ can be rewrote as

$$\begin{aligned} F_{ESC-tip} &= \frac{Q_s Q_t}{4\pi\varepsilon_0 Z^2} \\ &= -\frac{Q_s(Q_s + CV_{dc} + CV_{ac}\sin\omega t)}{4\pi\varepsilon_0 Z^2} \\ &= -\frac{Q_s(Q_s + CV_{dc}) + Q_s CV_{ac}\sin\omega t}{4\pi\varepsilon_0 Z^2} \\ &= \text{dc-term force} + \ \omega\text{-term force} \end{aligned}$$

Therefore, $F_{ESC\text{-}tip}$ is the function of dc-term force and ω-term force. The 2ω-term force $F_{2\omega}$ does not include the term $F_{ESC\text{-}tip}$.

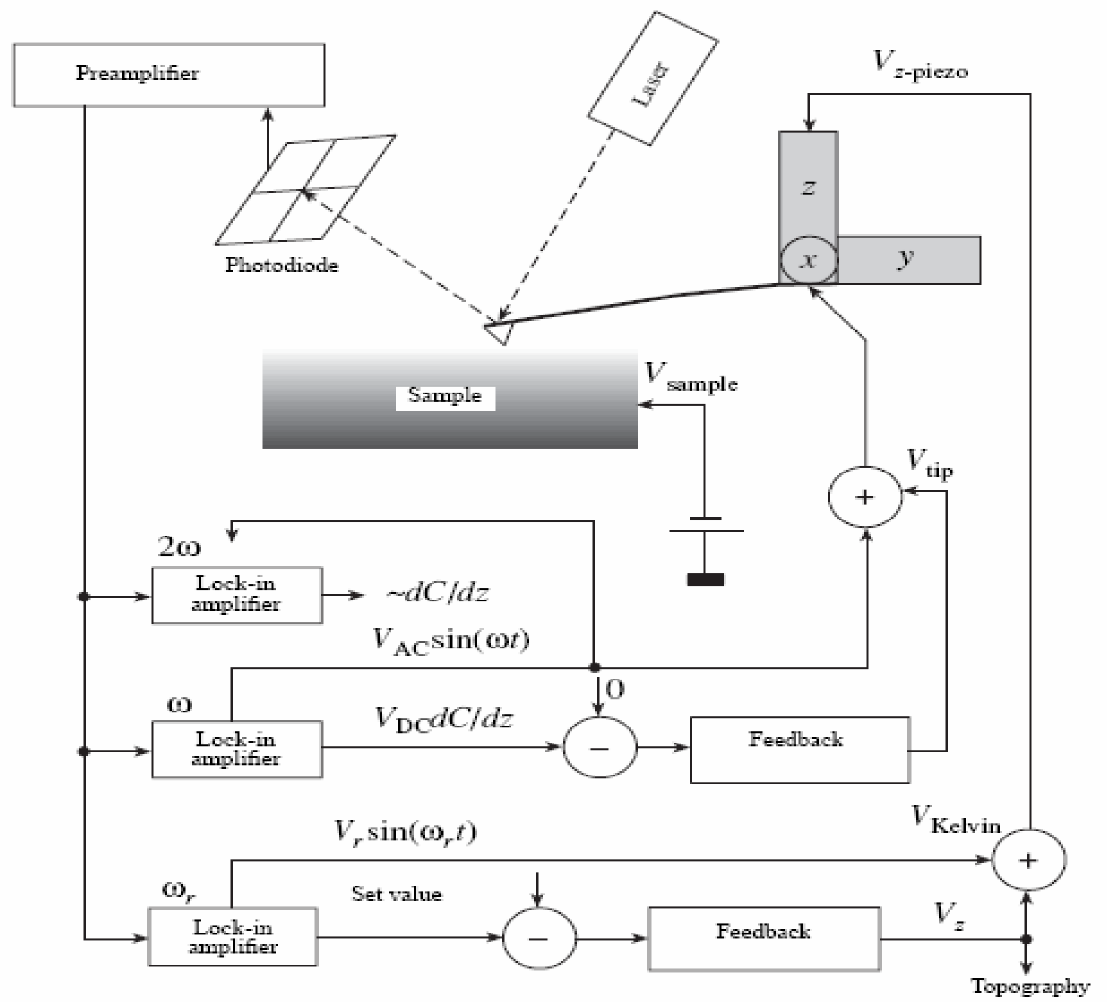

Fig. 2.2.1. Schematic diagram of scanning EFM. [2]

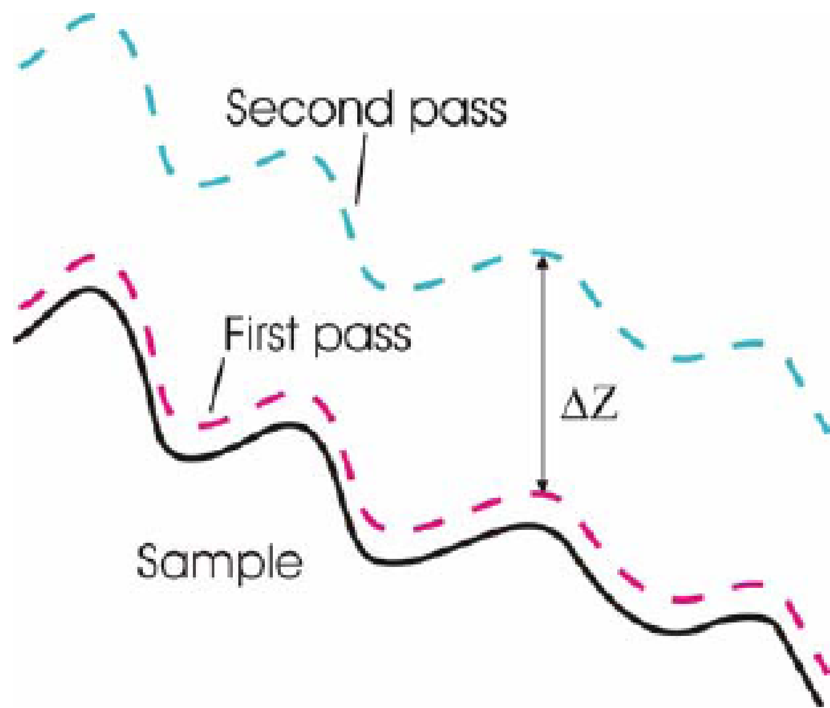

Fig. 2.2.2. Schematic diagram of two-pass method. (from NT-MDT Manual)

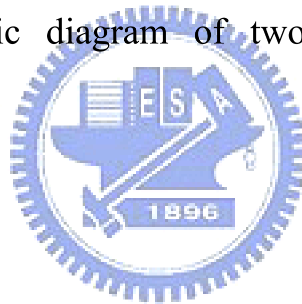

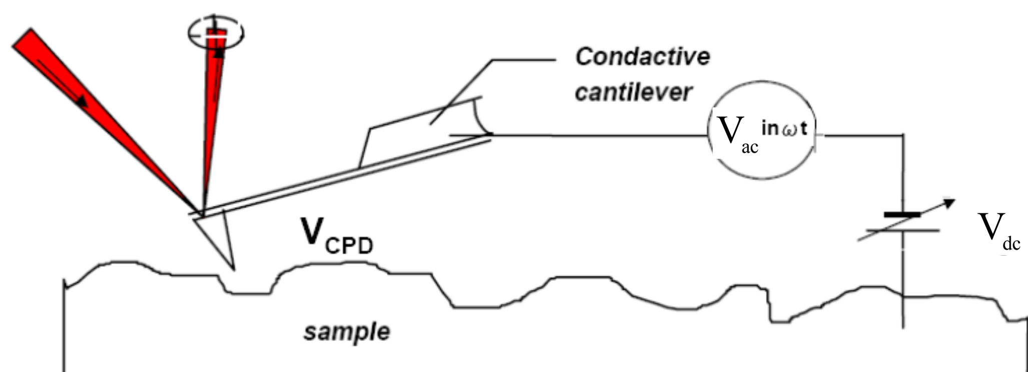

Fig. 2.2.3. Schematic diagram of biasd metal tip and sample. (from NT-MDT Manual)

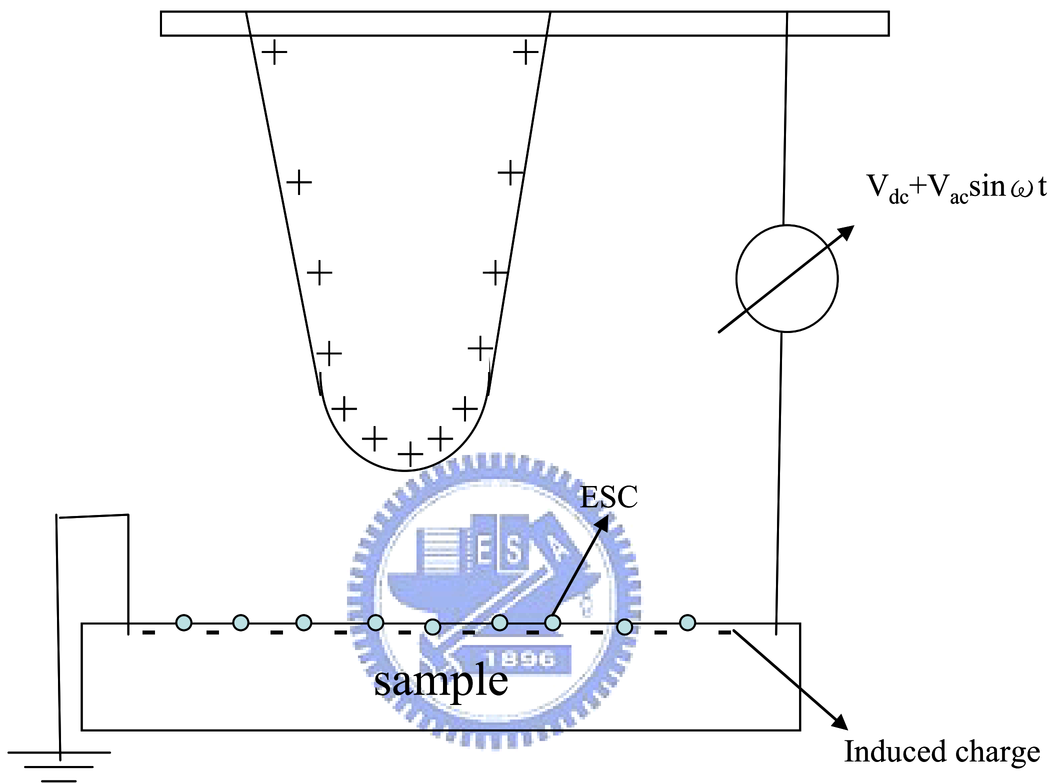

Fig. 2.2.4. Schematic diagram of biased metal tip and sample with surface electrostatic charge. The "+" and "-" are expressed as the induced charge resulted from the applied voltage. The circles on the sample are expressed as the surface electrostatic charge.

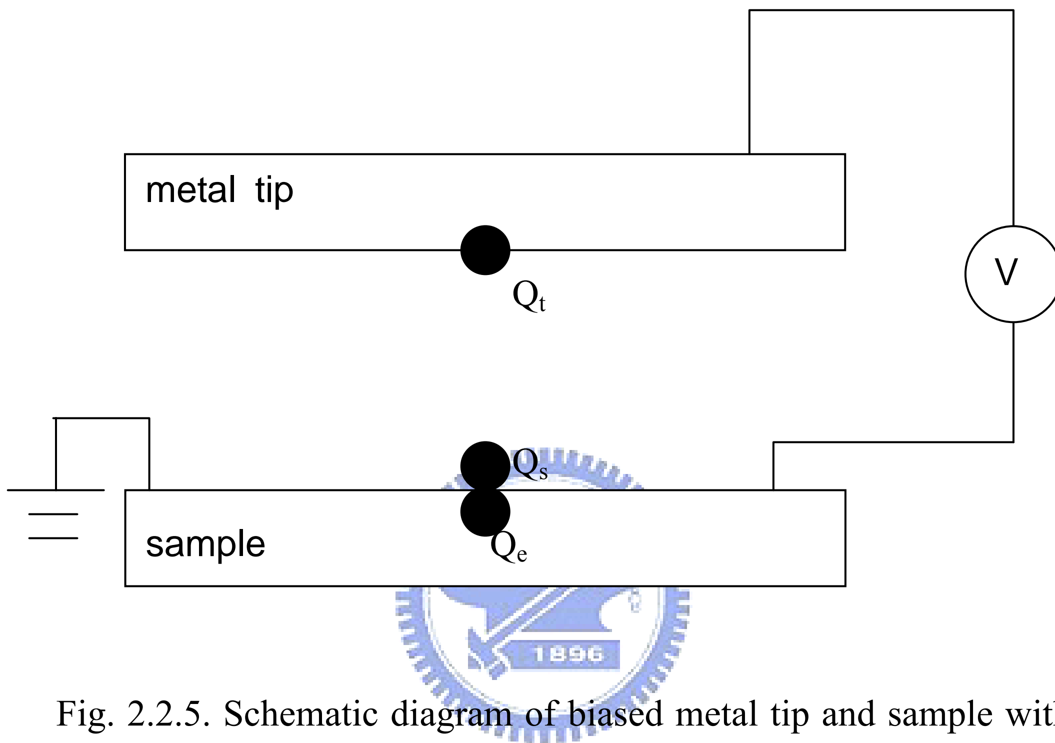

Fig. 2.2.5. Schematic diagram of biased metal tip and sample with surface electrostatic charge. This situation is regarded as parallel-plate model. The charges are regarded as point charges expressed by the solid circles.

2.3 Scanning Kelvin Probe Microscopy (SKM)

The SKM mode can be used to image distribution of surface potential on the sample surface. In SKM, we apply an AC and a DC voltage (V_{ac} and V_{dc} , respectively) simultaneously between the tip and sample, as shown in Fig. 2.2.3. At the same time, the SKM system monitors the cantilever vibration due to the electrostatic force at the fundamental frequency ω of the applied V_{ac}. As expressed by EFM formulas (Eq. (2-4)) in scanning EFM, the z-direction ω-term force acting on the tip is given as

$$F_{\omega} = -\frac{\partial C}{\partial Z}(V_{dc} - V_{CPD})V_{ac} + F_{ESC-tip,\omega} \tag{2-6}$$

For most of cases, the effect of Coulombic component $F_{ESC-tip,\omega}$ can be ignored, such that by tuning the V_{dc} to make F_{ω} to equal zero we can retrieved contact potential difference V_{CPD} which is equal to V_{dc} under this condition.

The operation of SKM is used in two-pass method, as similar to the case in scanning EFM. In the first scanning, we obtain the morphology image of sample surface. In the second pass, we obtain the mapping of variation of SKM feedback voltage on the same position at the sample surface.

Chapter 3　Experiments

In this chapter, the preparation of the samples, the experiment procedure, and the analysis instruments are described.

3.1 Sample Preparations

In our experiments, two sets of samples were used. The first series of samples were with flat surface, and the other set of samples possess micro structure on its surface. The first series of samples include intrinsic Si (i-Si) wafer, i-Si wafers coated with 200nm-Pt film and 200nm-Au film, respectively, using ion sputter (Hitachi E-1010). Their schematic diagrams of structure are shown in Fig. 3.1.1 (a).

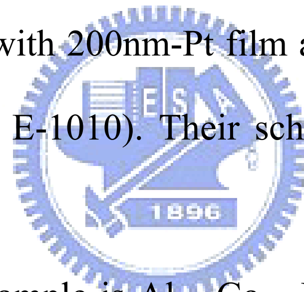
1896

The second type of sample is $Al_{0.11}Ga_{0.89}N$ epilayer with micro structures, GaN islands, grown by AIX 200/4 RF-S horizontal-reactor metalorganic chemical vapor deposition (MOCVD) system. Trimethylgallium (TMGa), trimethylaluminum (TMAl), and ammonia (NH_3) were used as the source precursors of Ga, Al, and N, respectively. Hydrogen was used as a carrier gas. Prior to the material growth, the sapphire substrate was heated to 1120℃ in a H_2 ambient for 10minutes to remove any residual impurities on the surface. The substrate was then cooled to 650℃ for the deposition of a nominal 25-nm-thick AlN nucleation layer. It followed by an increasing of substrate temperature to 1120℃ and then a growth of a 1.5 μm $Al_{0.11}Ga_{0.89}N$ layer.

Finally, the GaN islands were deposited at temperature 900℃ by the flow-rate modulation epitaxy (FME) technique. The schematic diagram of the sample structure is shown in Fig. 3.1.1 (b).

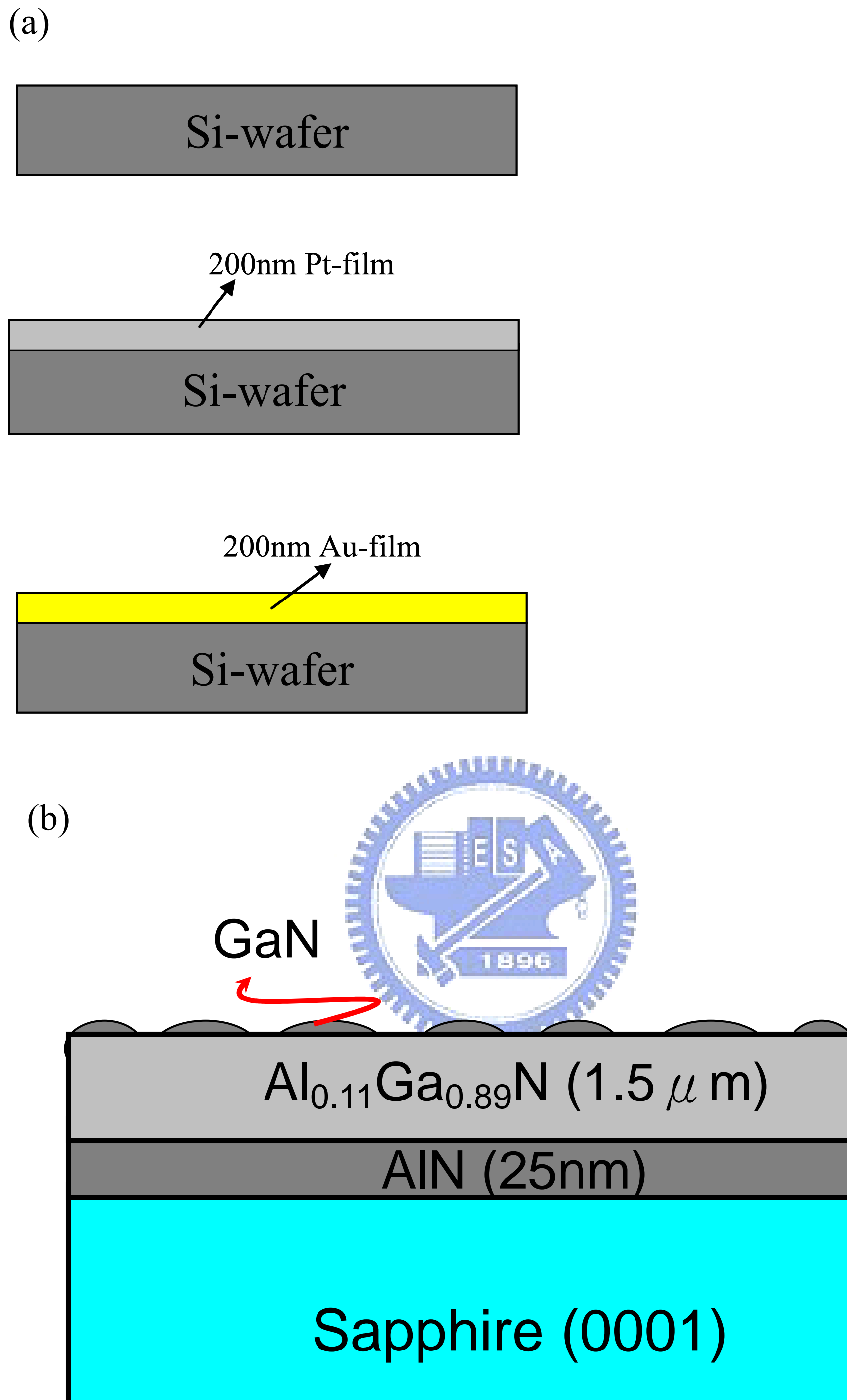

Fig. 3.1.1. Schematic diagrams of sample structure (a) Si wafer, Pt-coated Si wafer and Au-coated Si wafer, and (b) the sample with GaN islands.

3.2 Experiment Procedure

During the experiments, if clearing was necessary, the Si wafers were cleaned in the following procedures:

i. All of the Si wafers were dipped into the diluted BOE solution (HF: NH_4F=1:6) for 5 minutes to remove surface oxide. The diluted BOE solution was diluted with D.I. water and the concentration was about 10%.

ii. After removing the surface oxide, Si wafers were pulled out and blow-dried with N_2 gas.

iii. One of the Si wafer was put on the stage of SPM and made the measurement immediately to avoid surface oxidation. The other two Si wafer were put into the chamber of the ion sputter for coating 200nm-thick Au film and 200nm-thick Pt film on their surface, respectively.

iv. After coating, the Pt-coated Si wafer and Au-coated Si wafer were put on the stage of SPM and made the measurement immediately to avoid surface oxidation.

The schematic illustrations of grounding of the Si wafer and coated Si wafers on the SPM stage are shown in Fig. 3.2.1 (a).

Similarly, the GaN sample clearing procedure is as follows:

i. The sample was rinsed in the D. I. water whose resistance was larger than 15MΩ for two minutes to remove particles.

ii. The sample was dipped into the acetone (ACE) solution in ultrasonic cleaner and oscillated for 3 minutes to remove D. I. water.

iii. The sample was dipped into the isopropy alcohol (IPO) solution in ultrasonic cleaner and oscillated for 4 minutes to remove oil and organic pollution.

iv. The sample was rinsed in the D. I. water for 2 minutes to remove IPO.

v. The sample was dipped into the diluted hydrochloric acid (HCl) solution (HCl: H_2O=1:1) with D. I. water in ultrasonic cleaner and oscillated for 4 minutes to remove surface oxidation layer on the sample.

vi. The sample was rinsed in the D. I. water for 4 minutes to remove HCl and blow-dried with N_2 gas.

After the clearing, the sample was then put in the auto drybox for exceeding 1 hour to remove the moisture to a maximum extent. The sample on the stage of the SPM was grounded by putting In-ball film on the surface, as shown in Fig. 3.2.1 (b).

(a)

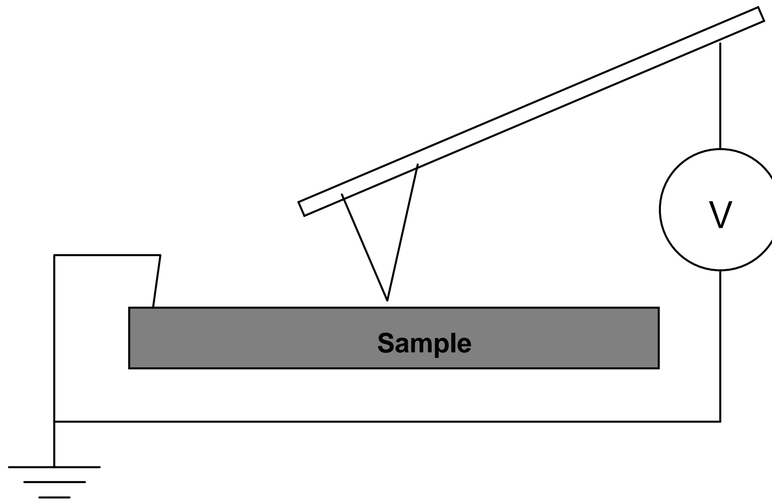

(b)

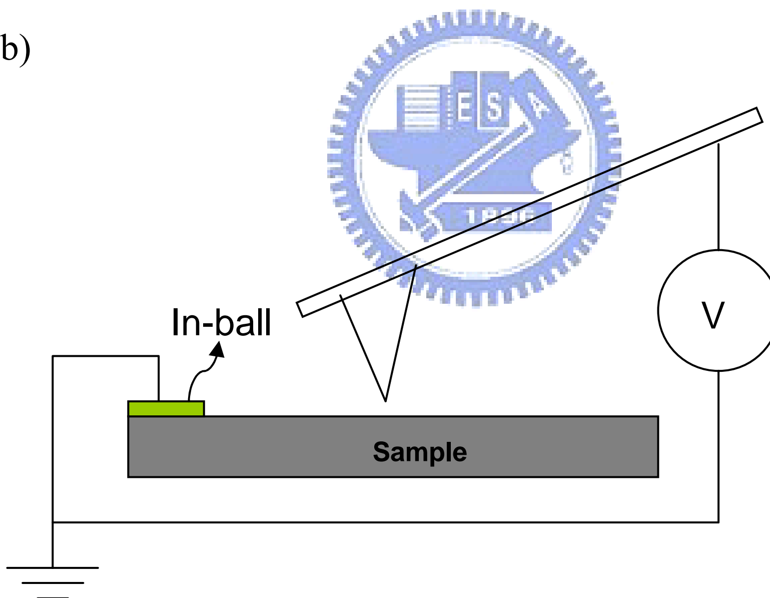

Fig. 3.2.1. Schematic diagrams of sample grounding of (a) Si wafer, Pt-coated Si wafer and Au-coated Si wafe, and (b) the sample with GaN islands.

3.3 Analysis Instruments

Our SPM system was manufactured by "Molecular Devices and Tools for Nano Technology "(NT-MDT Company) in Russia. The AFM system we used is Solver P47H that can be operated in multi-modes, such as AFM for morphology measurements, scanning EFM for ω-term and 2ω-term forces microscopy, SKM for the V_{CPD}, and lateral force microscopy for the friction distribution, conductive AFM for current mapping and I-V spectroscopy, MFM, etc. There are also many other functions in this system, such as force curve, force vs. applied voltage, etc. In our experiment, we operated the AFM, scanning EFM, and SKM in semi-contact mode. The latter two modes were operated in two-pass method to make the measurements at different tip-sample distances.

1896

The Si-probes used in this study were also from the NT-MDT. The conductive probes for SKM and scanning EFM were coated Pt film on the probe surface. They have a cantilever with length of 50 ~ 80 μm. The sharp tip have nominal radius of curvature of 10~30 nm, height of about 15 μm and the cone angle of about 25°. The SEM image of probe is shown in Fig. 3.3.1.

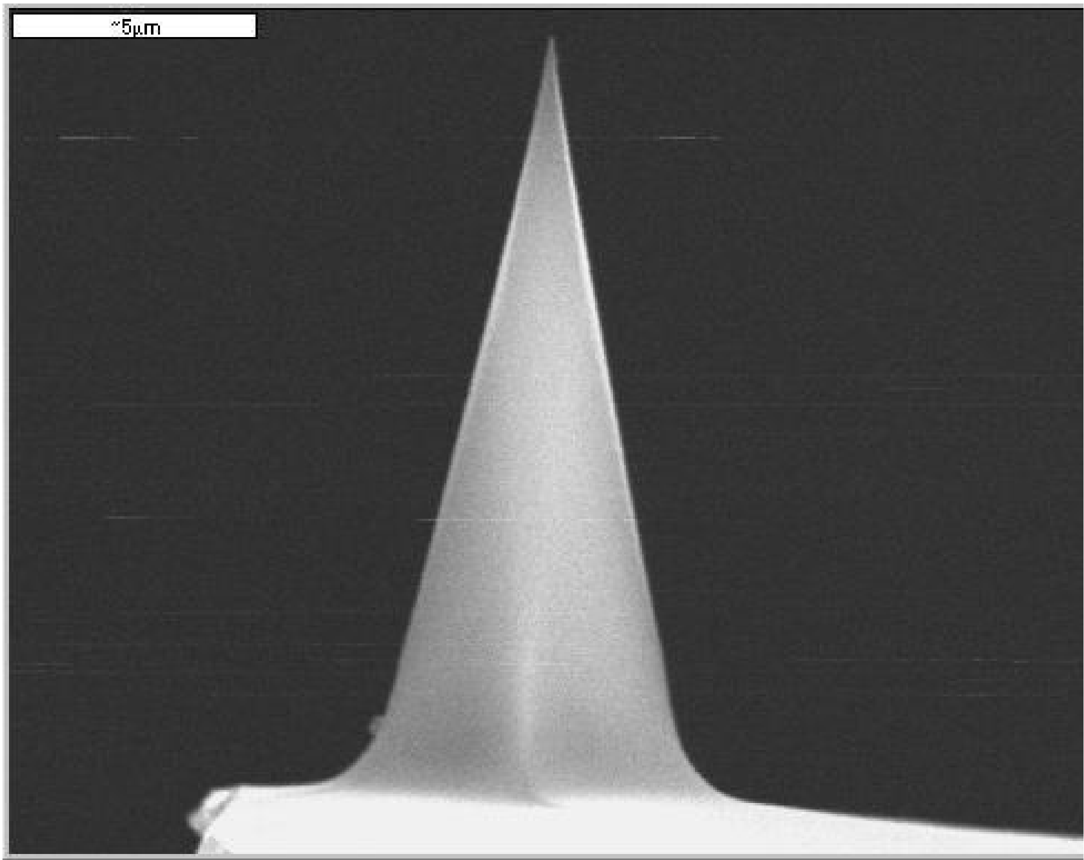

Fig. 3.3.1. SEM image of the probe.

Chapter 4 Results and Discussion

In this chapter, we present experimental results and a proposed model to describe them. Firstly, we introduce the model used here. Secondly, we show how to calibrate the work function of metal-coated tip by comparing the results with the theoretical calculation. Finally, we show the tip to sample distance dependence of the ω- and 2ω-force acting on the tip, which the forces originate from the surface ESC on the samples with flatness and with a single disk-like GaN island, respectively, and propose explanation for the experimental results.

4.1 Model

We measured the ω- and 2ω-force at different tip-sample distances, respectively. Thus, the Eq. (2-4) and (2-5) can be rewrote as the following equations:

$$F_{\omega}(Z) = -\frac{\partial C(Z)}{\partial Z}(V_{dc} - V_{CPD})V_{ac} + F_{ESC-tip,\omega}(Z) \tag{4-1}$$

$$F_{2\omega}(Z) = \frac{1}{4}\frac{\partial C(Z)}{\partial Z}V_{ac}^{2} \tag{4-2}$$

where Z is the tip to sample distance. The other parameters, V_{dc} and V_{ac}, were kept constant during the experiment, whose values were under 1 volt for V_{dc} and fixed 0.1 volt for V_{ac}. The value of Z was obtained from force curve in the first pass of AFM system.

It is noted that the Eq. (4-1) consists of capacitive component (first term)

and Coulombic component (second term). We found that the Coulombic component has many expressed forms in the published literatures. The Coulombic component has been treated as the interaction between point-charges [17-22], charged plates [24-25], as well as point-charge and charged plate [26-31]. In our studies, we would merely analyze the tip-sample distance dependence of the ω-term Coulombic force . So, we wrote it as the form $F_{ESC-tip,\omega}(Z)\cdot$

Moreover, it is also noted that the origin of the capacitance C which is considerably important in the term $\partial C/\partial Z$ in the Eq. (4-1). It is usually presumed [27, 32-36] that the capacitance value is independent of the shape and charge distribution of the tip and cantilever. That is the total capacitance C can be simply the sum of the capacitance components between the tip and the sample (C_{tip}) as well as between the cantilever and the sample (C_{canti}). The total capacitance is given as

$$C = C_{tip} + C_{canti}$$

In a typical SPM setup, the cantilever to sample distance (>15μm) is much larger than the tip to sample distance (~tens to hundreds of nanometers). The maximum vibration magnitude of the tip in the distance, about 10nm, is much less than the tip length L. Since, the electrostatic force changes as L^{-2}, we can expect that the variation of cantilever capacitance (C_{canti}) is less than 0.3%, and can be negligible. Thus, it comes to a conclusion that the main contribution of electrostatic force to the reduction in $\partial C/\partial Z$ is due to the tip-sample

interaction: [34-35]

$$F = F_{canti} + F_{tip} \approx F_{tip}$$

By rearrangement of Eq. (4-2), we have

$$\frac{\partial C(Z)}{\partial Z} = \frac{4F_{2\omega}(Z)}{V_{ac}^2} \qquad (4\text{-}3)$$

Because V_{dc} and V_{ac} were known and V_{CPD} could be obtained from SKM measurement when $Z > 4\mu m$, by substituting Eq. (4-3) into Eq. (4-1), we can extract the dependence of $F_{ESC-tip,\omega}(Z)$ on tip-sample distance, as shown in the following

$$F_{ESC-tip,\omega}(Z) = F_{\omega}(Z) + \frac{4F_{2\omega}(Z)}{V_{ac}}(V_{dc} - V_{CPD}) \qquad (4\text{-}4)$$

Through this method, we can acquire the tip to sample distance dependence of the forces $F_{ESC-tip,\omega}(Z)$ at low tip-sample distance.

4.2 Calibration of work function of tip

According to the SKM principle, we know that the value of CPD is the difference of work function between sample surface and metal-tip surface. [14, 16] We used the Pt-coated tip in our experiments. Since the Pt-coated film is rather than 10nm and tends to oxidize easily, we would confirm the work function of the metal-tip surface in the first place. In G. Koley's phrase, the saturated feedback voltage V_{dc} (marked as "region of measurement" in Fig. 1.1) can be regarded as the CPD because the Coulombic component becomes negligible at this distance range.

The Fig. 4.2.1 (a) and (b) show the AFM image and SKM mapping of Si wafer at constant distances between the tip and the Si wafer. The SKM signal increases much rapidly with the increasing value of distance for $Z<\sim 1\mu m$ and varies slowly when $Z>\sim 2\mu m$, which is similar to the result of G. Koley *et al*. To get a better signal-to-noise ratio, the SKM signal is extracted by averaging over the same square region (~2μm × ~2μm). We measured the SKM signals of Si wafer, 200nm-thick Pt-film/Si wafer, and 200nm-thick Au-film/Si wafer at different distance from ~100nm to ~4μm, as shown in Fig. 4.2.2. We found the SKM signals would be saturated at the distances $>\sim 2\mu m$. It is worth to remind that the saturated value of V_{dc} represents the value of V_{CPD} between metal tip and sample. The experimental data indicates that the V_{CPD} for i-Si, Au-coated and Pt-coated Si wafers are 0.603V, 0.046V, and -0.442V, respectively. For comparison, the relationship between the value of CPD (V_{CPD}) and the work

function of various metals are also indicated in Fig. 4.2.3. According to the definition of V_{CPD} [14]:

$$eV_{CPD} = \Phi_{tip} - \Phi_{sample} \tag{4-5}$$

where Φ_{tip} and Φ_{sample} are the work function of tip surface and sample surface, respectively. And the work function of i-Si, Au, and Pt are 4.6eV [37], 5.1eV [38], and 5.65eV [38]. The derivative of eV_{CPD} to Φ_{sample} is exactly equal to -1 theoretically. The slope of the fitted linear line of our experimental results is about –0.99 which is very close to the predicted value. It shows the data in this series of measurements is correct in substance.

From Fig. 4.2.4, we can derived the work function of the Pt-coated tip from the contact potential difference V_{CPD} between Pt tip and Si wafer, and later on obtain the work function of other samples using the same tip via the above measurement of V_{CPD}.

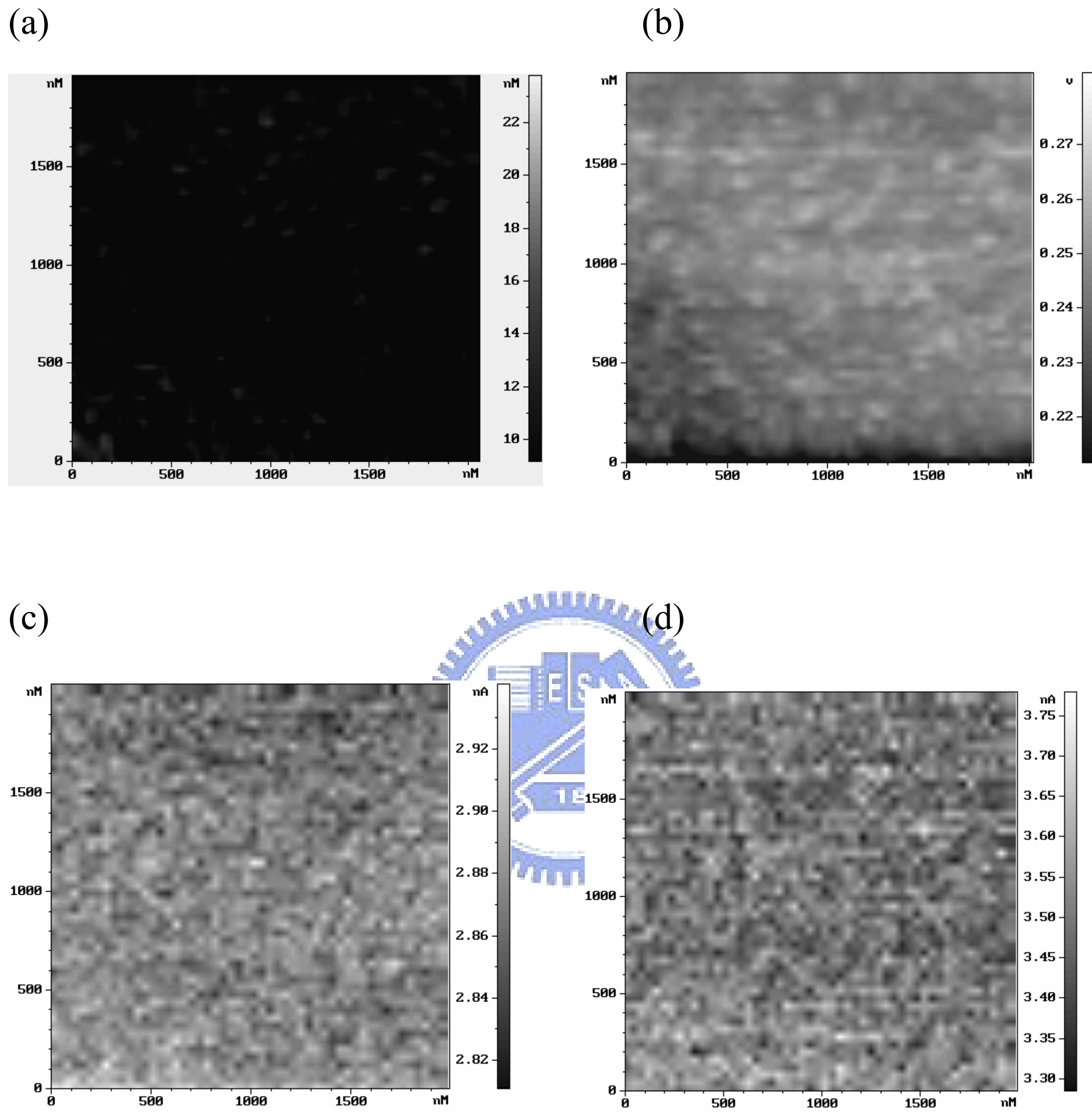

Fig. 4.2.1. (a) The AFM of Si wafer surface. (b) The SKM mapping, (c) the ω-force mapping, and (d) the 2ω-force mapping are the same region as the AFM image (a) on the Si wafer. Their value are obtained by averaging over the same square region (~2μm × ~2μm) for improvement of signal to noise ratio.

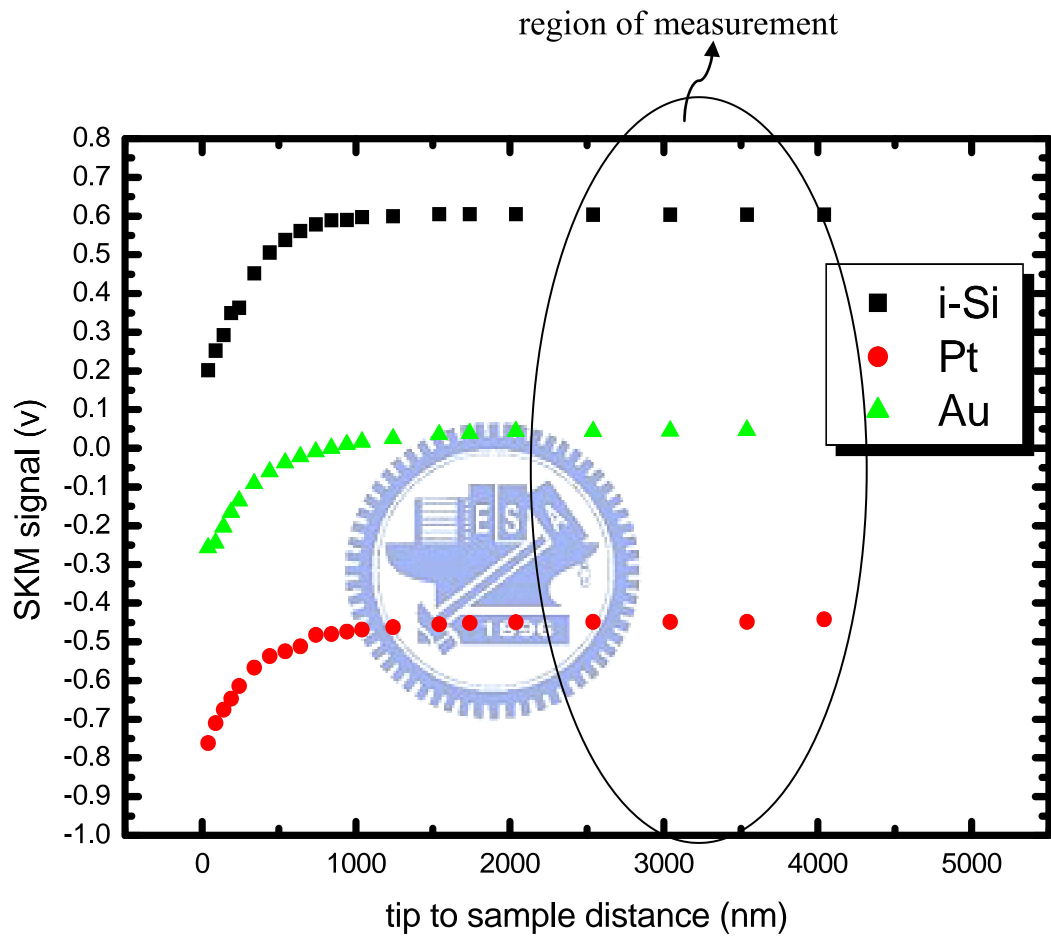

Fig. 4.2.2. The SKM signal vs. tip to sample distance for i-Si, 200nm-Pt/Si, and 200nm-Au/Si. When the distance is larger than 2000nm, the SKM signals of the samples tend to a constant, respectively.

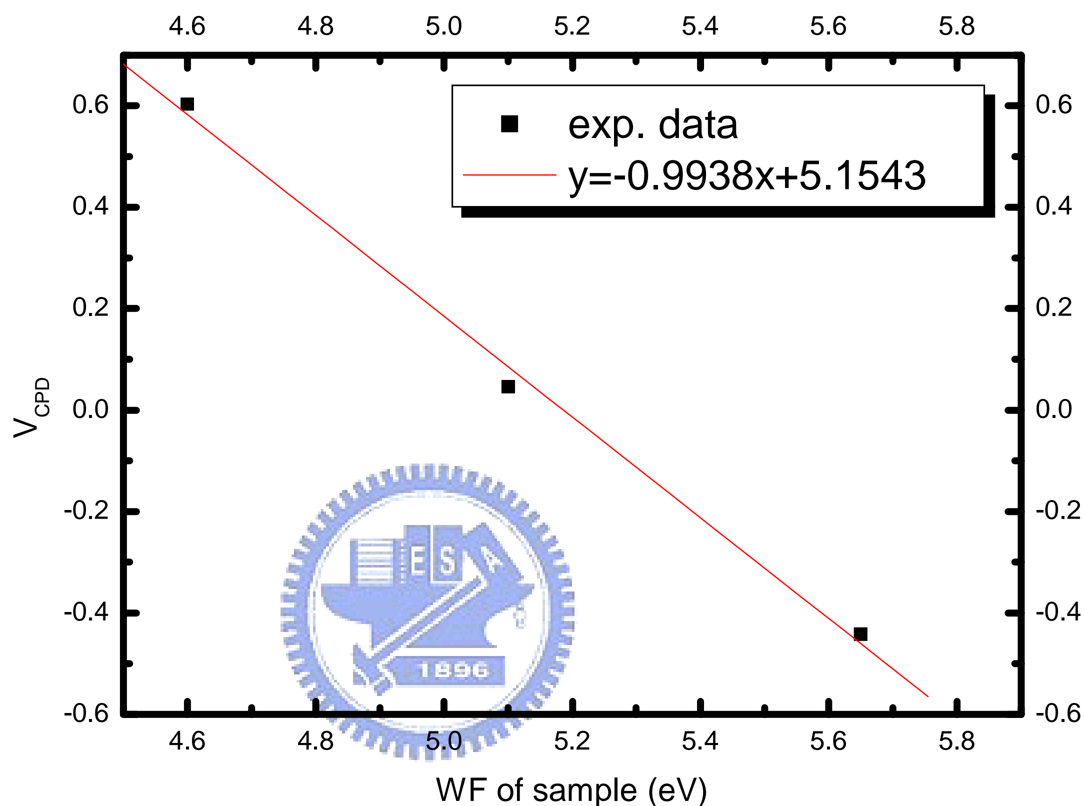

Fig. 4.2.3. Relationship between V_{CPD} and work function. The dots express the saturated feedback voltage values (SKM signals) in Fig. 4.2.2. The slope of the fitted linear line is about -0.99 which is very close to the theoretical result, -1.

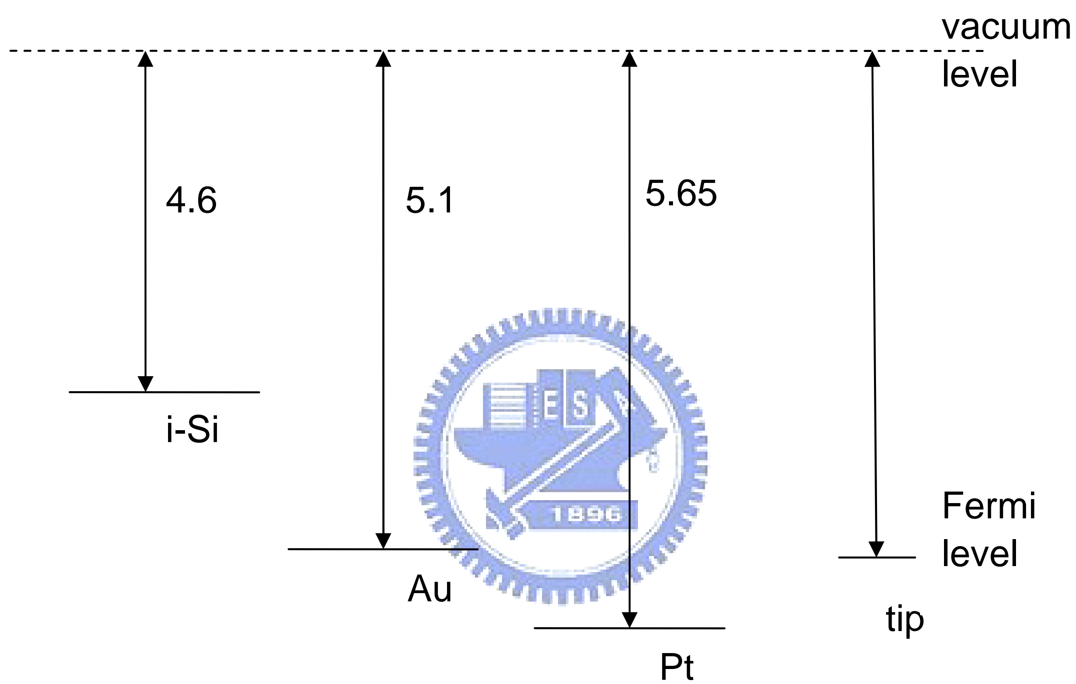

Fig. 4.2.4. Schematic diagram of work function of different samples and metal tip.

4.3 ω-$F_{ESC\text{-}tip}$ from plane on sample

We also studied the scanning EFM on the Si wafer. The experimental values were extracted from the mapping (as shown in Fig. 4.2.1 (c) and (d)) in the same method as the SKM signal, mentioned in section 4.2. Figure 4.3.1 shows the tip-sample distance dependence of ω-force and 2ω-force acting on the tip from Si wafer, respectively. We found that the intensity of both forces decrease with the increasing tip-sample distance. Based on the model as mentioned in section 4.1 and Eq. (4-4), we can obtain the electrostatic force $F_{ESC-tip,\omega}(Z)$ between the tip and the surface ESC on Si wafer, as shown in Fig. 4.3.2.

For scanning EFM, the tip surface was more adequately described as a hyperboloidal surface due to the fact of smaller tip-sample distance used here in the range of hundreds of nanometers, it is more proper to employ the cone model [39] (Fig. 4.3.3) to describe the experimental results. The formula of electrostatic force of cone model is expressed as [39]

$$F = 4\pi\varepsilon_0 V_b^2 \left[\frac{\ln\left[1+\left(r_{max}/R\right)^2 (1+\frac{R}{Z})\right]}{\ln^2\left[\frac{1+\eta_{tip}}{1-\eta_{tip}}\right]} \right] \quad (4\text{-}6)$$

where V_b is the applied voltage on the tip, R is the tip radius and $\eta_{tip} = \sqrt{Z/(Z+R)}$.

We used the Eq. (4-6) to fit the data of $F_{ESC-tip,\omega}(Z)$ calculated from Fig.

4.3.1 and Eq. (4-4) by tuning three parameters which were the radius R, the length L and the half cone angle θ of the tip, as showing in Fig. 4.3.4, and $r_{max} \approx L \tan\theta$. The fitted result indicated that the radius R is about 10nm, the length L is about 14μm, and the cone angle is about 27° of the tip we used in this measurement, as shown in Fig. 4.3.2. These values agree well with the specification of the probe (R=10~30nm, L~15μm and cone angle ~25°) from NT-MDT Company and our SEM image (as shown in Fig. 3.3.1). In our experiment, the Si wafer is a square with an area of 1 cm^2, which is much larger than the apex area (~400nm^2). Thus, our Si wafer could be treated as the infinite plane for the tip. In such a way, we can obtain the $F_{ESC-tip,\omega}$ by assuming the surface ESC on the infinite semiconductor plane based on cone model.

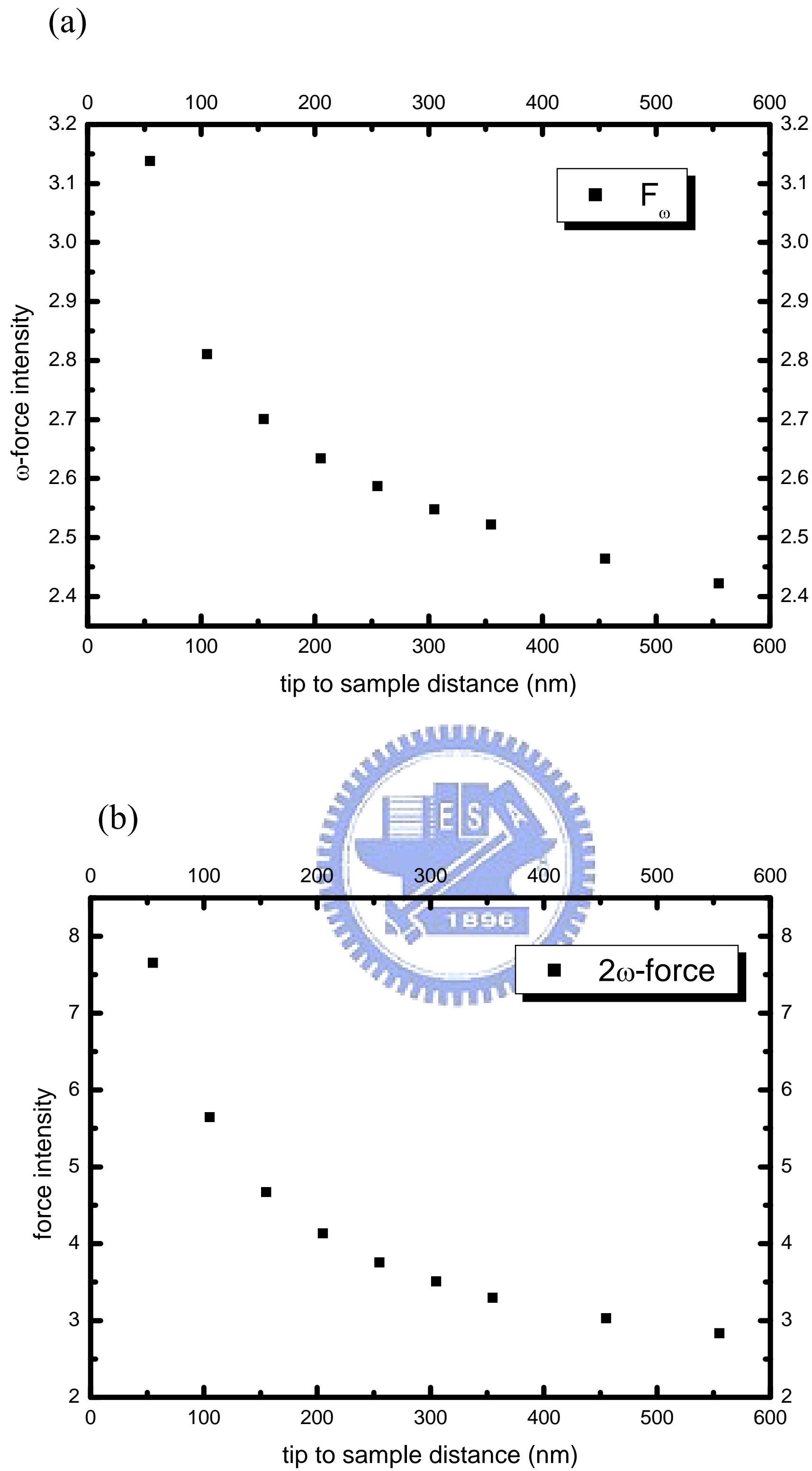

Fig. 4.3.1. The experimental results of (a) ω-force and (b) 2ω-force intensities vs. tip to sample distance.

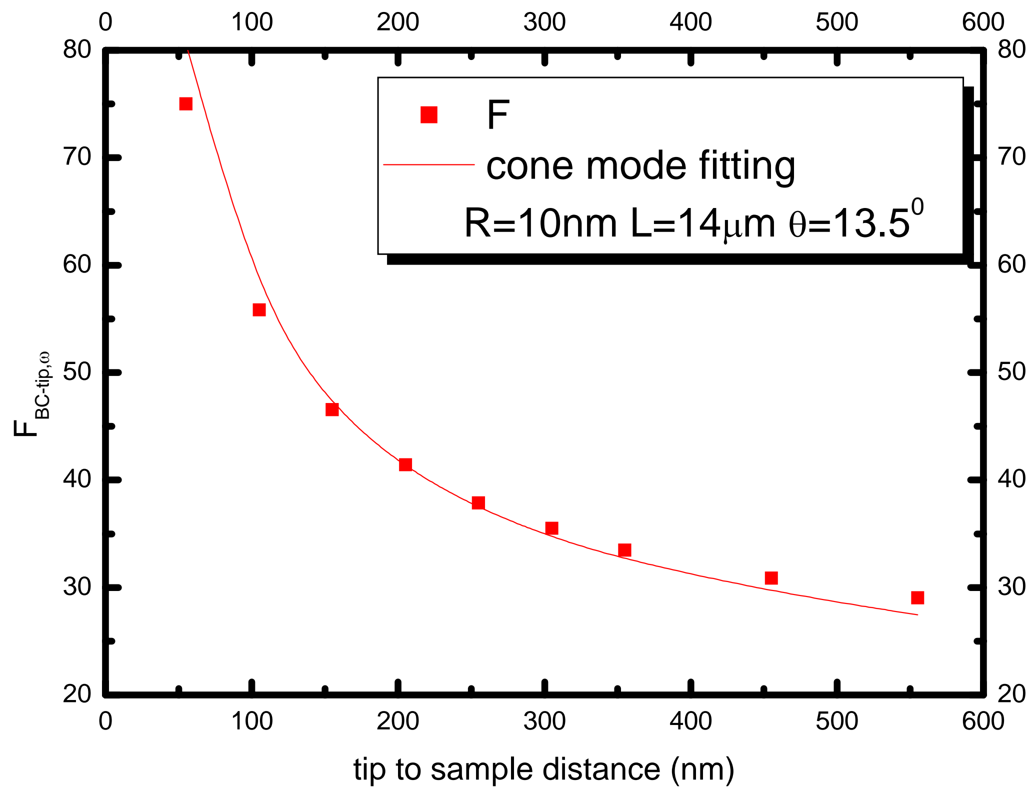

Fig. 4.3.2. The experimental data (marked in square dots) and fitted result (curve) of the $F_{ESC-tip,\omega}(Z)$ intensity vs. the tip-sample distance.

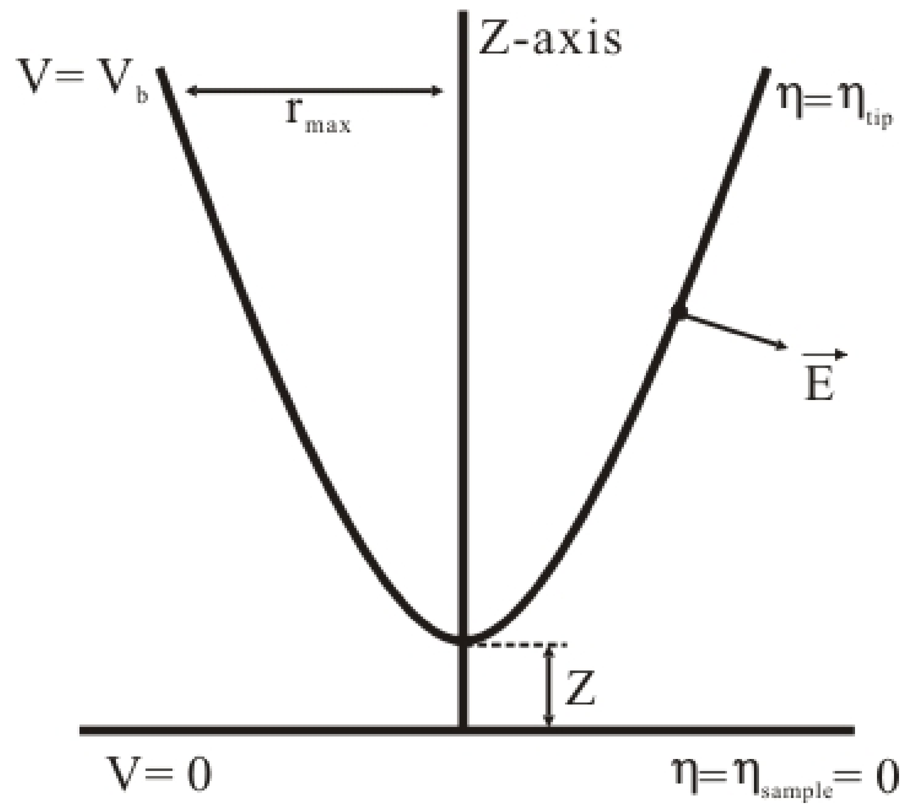

Fig. 4.3.3. Schematic diagram of cone model. [39]

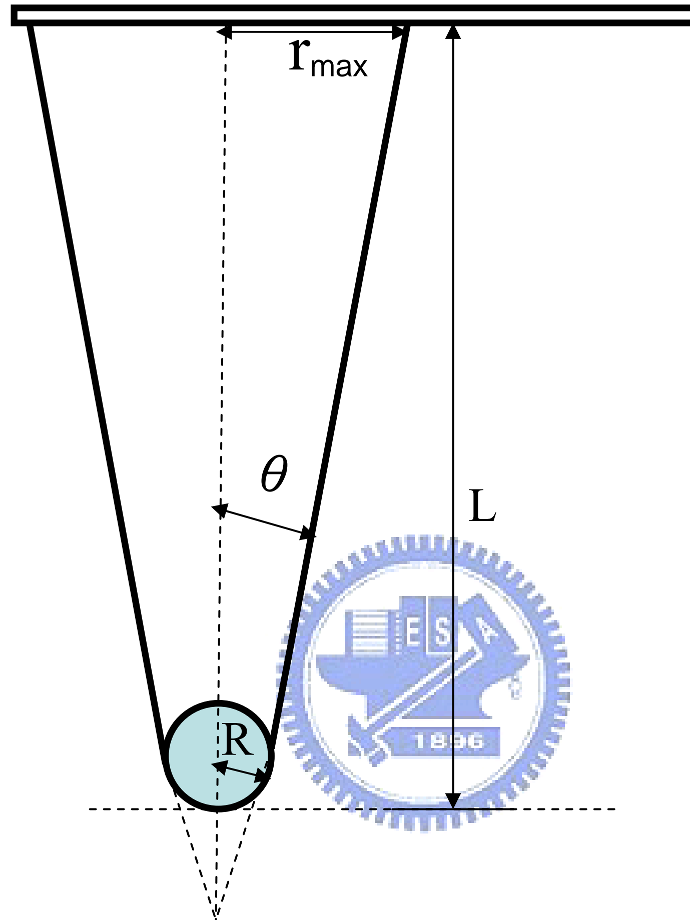

Fig. 4.3.4. Schematic diagram of tip mounted on the probe.

4.4 Morphology and force mapping of GaN island

Next, we used the same technique in the sample with GaN disk-like islands. We would analyze the ω-term force acting on the tip from the single island. In the first place, we observed the shape of the GaN island in this section.

Figure 4.4.1 shows the 5μm × 5μm AFM plane-view image of the GaN sample grown on $Al_{0.11}Ga_{0.89}N$/sapphire (0001) substrate. The estimated dot density is about $2.3\times10^8/cm^2$. The height is ranged from 2nm to 15nm and the average value is about 5.7nm with standard deviation of 2.1nm. The diameter is ranged from ~100nm to ~400nm and the average value is about 175nm. The aspect ratio (height/diameter) is ranged from 1/13 to 1/50 and the average value is about 1/30. The shape of the single GaN island is disk-like, as shown in Fig. 4.4.2.

Figure 4.4.3 shows the ω-force mapping (a)-(b) and 2ω-force mapping (c)-(d) of GaN islands, respectively. GaN islands are also well resolved in both the ω-force and 2ω-force images as shown in Fig. 4.4.3 (b) and (d), respectively. It is also seen in the profiles of morphology and force intensity as shown in Fig. 4.4.4. The profiles of surface morphology and ω-force along the dotted line in Fig. 4.4.3 (a)-(b) are shown in Fig. 4.4.4 (a) and (b). The profiles of surface morphology and 2ω-force along the dotted line in Fig. 4.4.3 (c)-(d) are shown in Fig. 4.4.4 (c) and (d). It is interesting to note that the profiles of the ω-force and 2ω-force mapping images are gentle similar. For the case of GaN islands the higher the island is, the lower the magnitude of electrostatic force (F_{ω} and $F_{2\omega}$)

can be obtained.

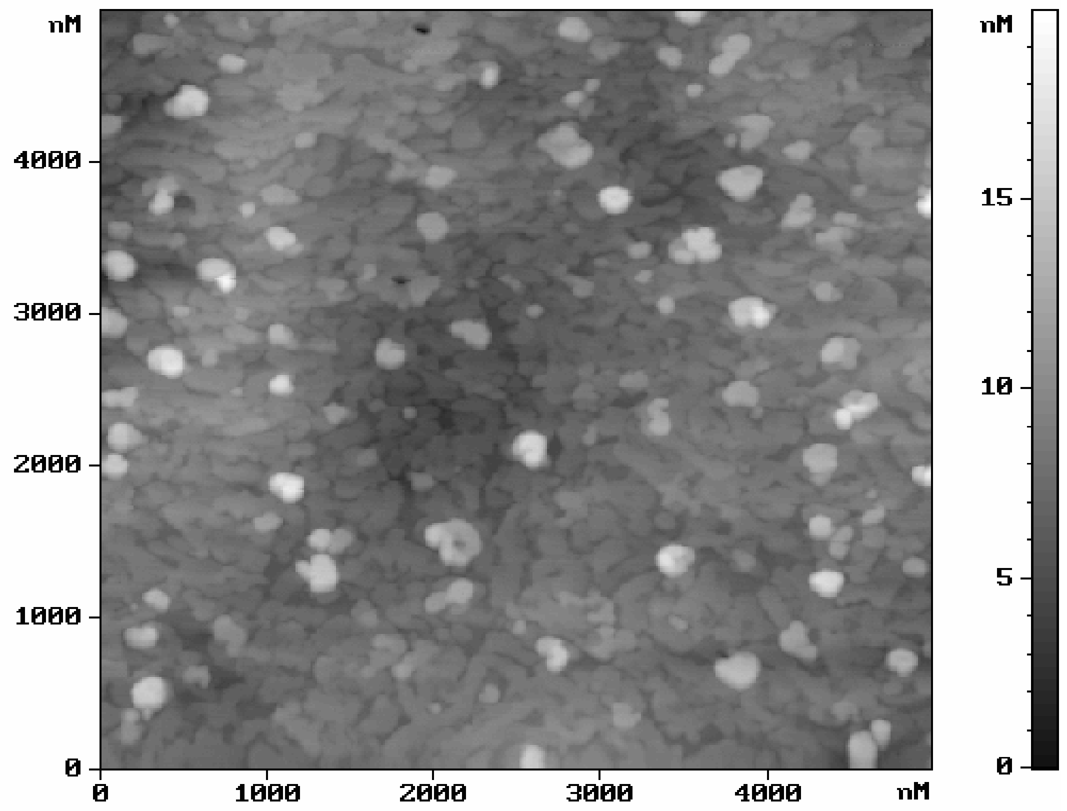

Fig. 4.4.1. The plane view image of AFM scan on the GaN islands.

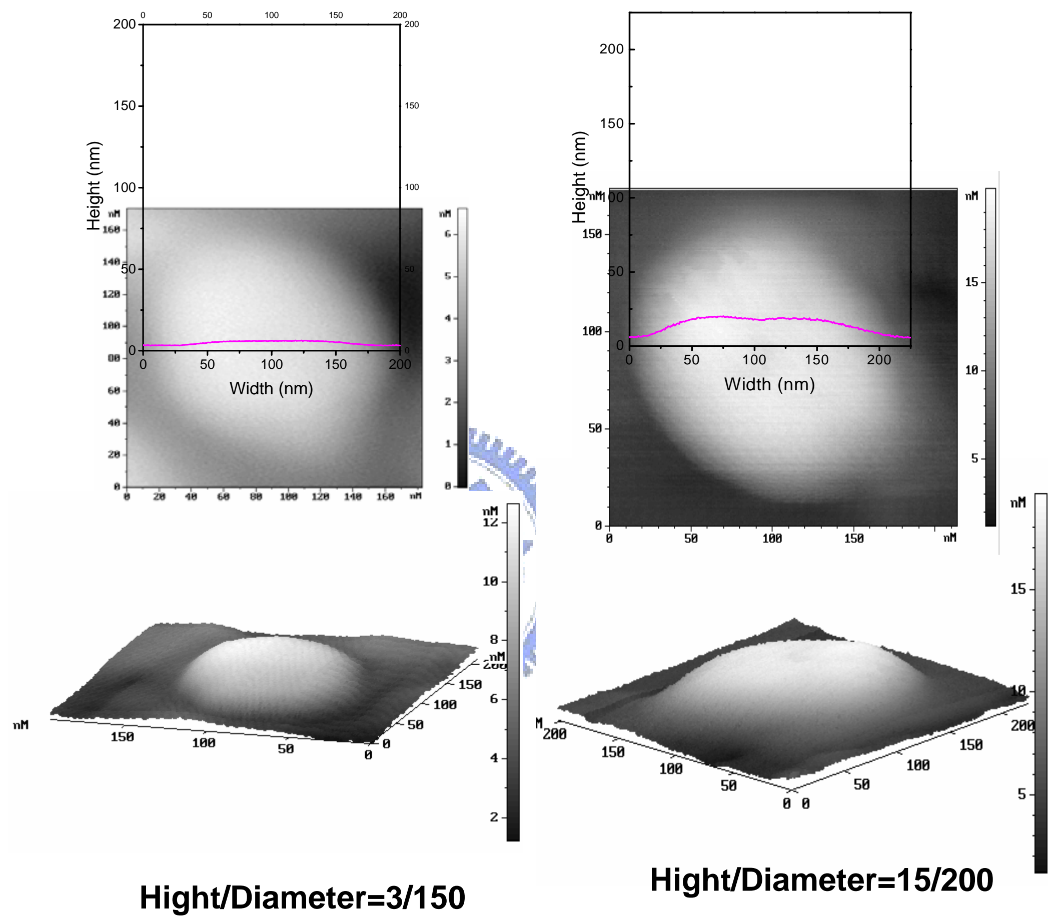

Fig. 4.4.2. The AFM 2-D and 3-D images of the single GaN island. The inset figures in the 2-D images are their profiles, respectively.

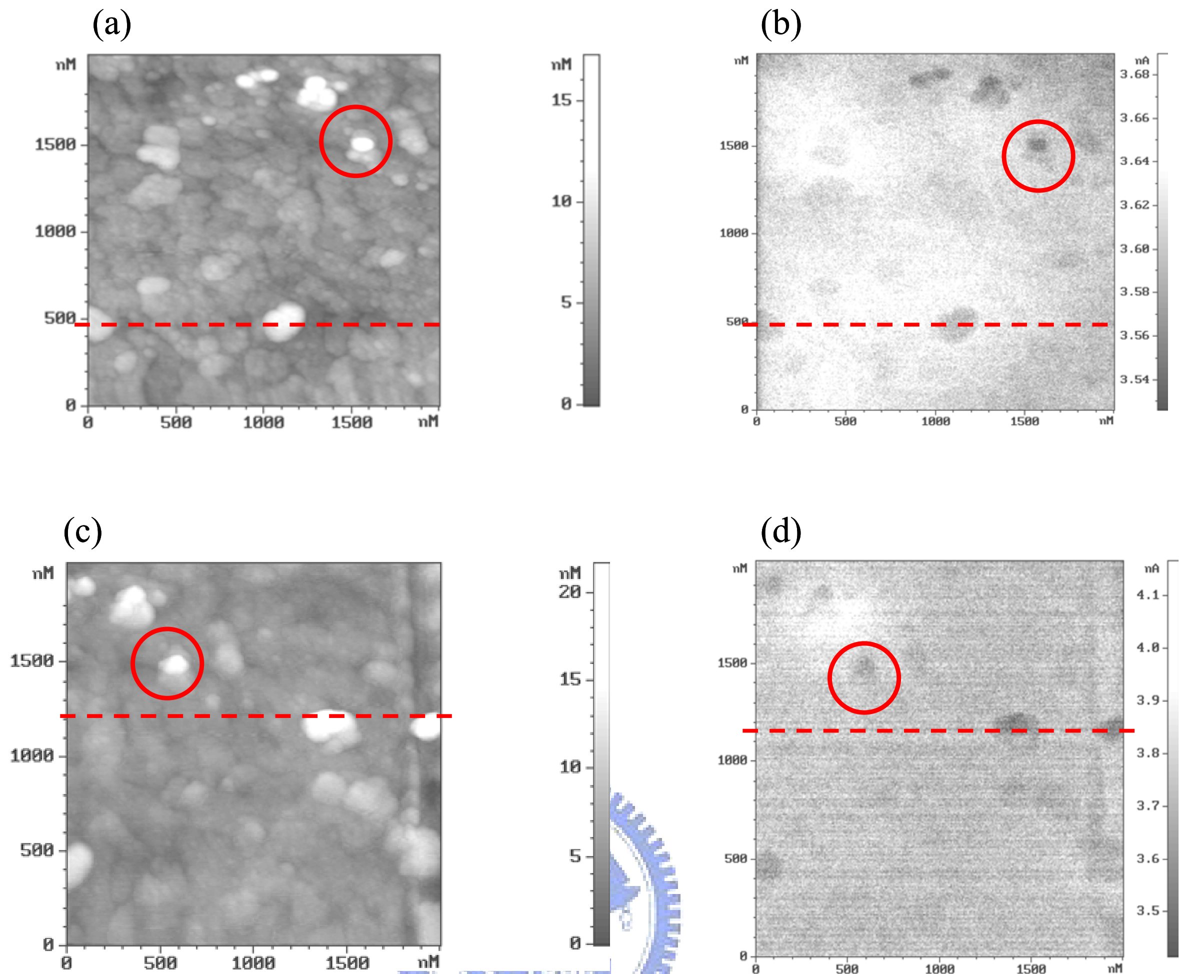

Fig. 4.4.3. The AFM image (a) and the relative ω-force mapping (b) of GaN islands. The AFM image (c) and the relative 2ω-force mapping (d) of another portion of GaN islands.

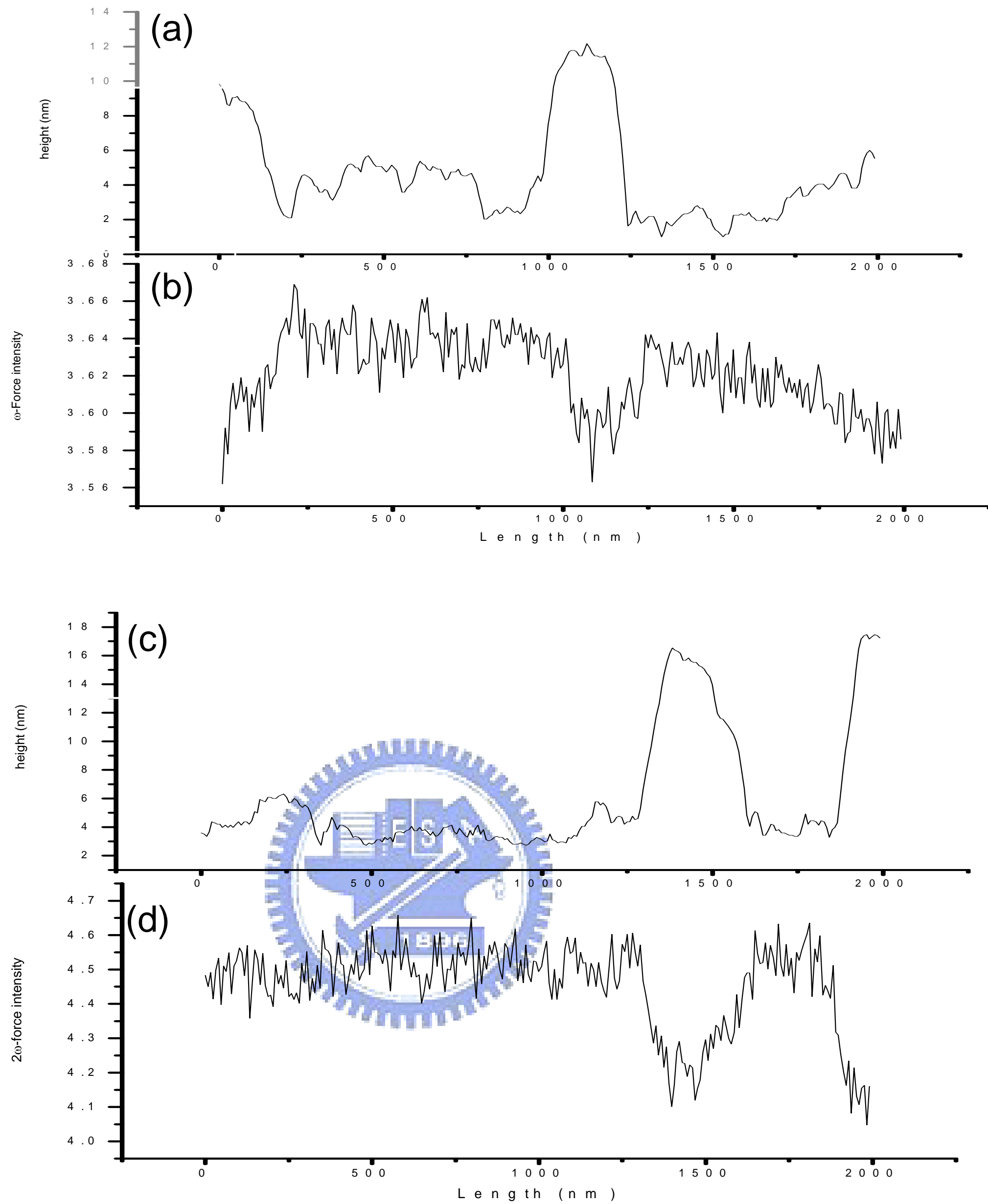

Fig. 4.4.4. (a) and (b) are the height profile and their contrast ω-force intensity profile, respectively, located along the dotted line on Fig. 4.4.3 (a)-(b). (c) and (d) are the height profile and their contrast 2ω-force intensity profile, respectively, located along the dotted line on Fig. 4.4.3 (c)-(d).

4.5 ω-$F_{ESC\text{-}tip}$ from the single GaN island

In this section, we would discuss the tip-sample distance dependence of the ω-force acting on the tip from the surface charge on the fixed GaN island. The sample is AlGaN epilayer with GaN islands and its morphology is shown in Fig. 4.4.3. When the tip is above the fixed island during the scanning, we believed that the ω-force acting on the tip, F_{ω}, consists of two parts. One is the ω-force between the tip and the island, $F_{tip\text{-}is,\omega}$, and the other is the ω-force between the tip and the entire plane area except of island itself, $F_{tip\text{-}p,\omega}$. And they both consist of capacitive and Coulombic components, respectively. Thus, the ω-force acting on the tip can be expressed as the sum of the two kinds of ω-forces: (see Fig. 4.5.1)

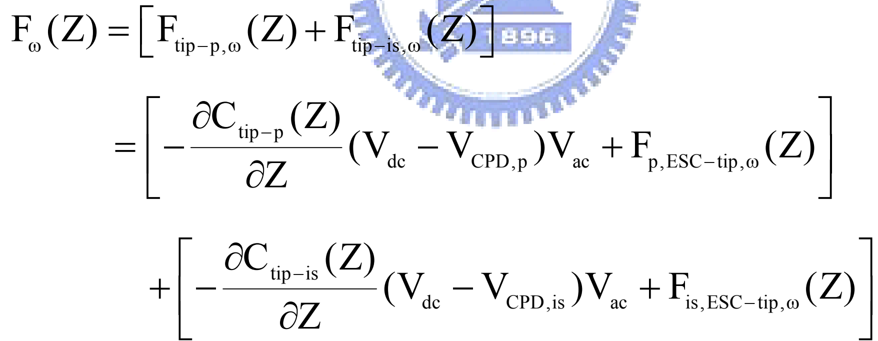

$$
\begin{aligned}
F_{\omega}(Z) &= \left[F_{tip-p,\omega}(Z) + F_{tip-is,\omega}(Z)\right] \\
&= \left[-\frac{\partial C_{tip-p}(Z)}{\partial Z}(V_{dc} - V_{CPD,p})V_{ac} + F_{p,ESC-tip,\omega}(Z)\right] \\
&\quad + \left[-\frac{\partial C_{tip-is}(Z)}{\partial Z}(V_{dc} - V_{CPD,is})V_{ac} + F_{is,ESC-tip,\omega}(Z)\right]
\end{aligned}
$$

where $F_{tip\text{-}p,\omega}$ is the ω-force between the tip and the plane, $F_{tip\text{-}is,\omega}$ is the ω-force between tip and the specific island, $F_{p,ESC\text{-}tip,\omega}$ is the ω-term Coulombic force between the tip and the surface ESC on the plane, $F_{is,ESC\text{-}tip,\omega}$ is the ω-term Coulombic force between tip and the surface ESC on the specific island, and $V_{CPD,p}$, $V_{CPD,is}$, $C_{tip\text{-}p}$, $C_{tip\text{-}is}$ denote the V_{CPD} on the plane around the specific island, the V_{CPD} on the specific island, the capacitance between the tip and the

plane around the specific island, and the capacitance between the tip and the specific island, respectively. In the experiment, when the applied dc voltage $V_{dc}= V_{CPD,p}$, the capacitive term of the island can be neglected. Thus, we can have an equation with a much simple form, and obtain the Coulombic force between tip as well as the surface ESC on the specific island, $F_{is,ESC-tip,\omega}$, by the following equation.

$$
\begin{aligned}
F_{\omega}(Z) &= \left[-\frac{\partial C_{tip-p}(Z)}{\partial Z}(V_{dc}-V_{CPD,p})V_{ac} + F_{p,ESC-tip,\omega}(Z) \right] \\
&+ \left[-\frac{\partial C_{tip-is}(Z)}{\partial Z}(V_{dc}-V_{CPD,is})V_{ac} + F_{is,ESC-tip,\omega}(Z) \right] \\
&\approx \left[-\frac{\partial C_{tip-p}(Z)}{\partial Z}(V_{dc}-V_{CPD,p})V_{ac} + F_{p,ESC-tip,\omega}(Z) \right] + F_{is,ESC-tip,\omega}(Z) \\
&= F_{tip-p,\omega}(Z) + F_{is,ESC-tip,\omega}(Z) \\
F_{is,ESC-tip,\omega}(Z) &= F_{\omega}(Z) - F_{tip-p,\omega}(Z)
\end{aligned}
\tag{4-7}
$$

We conducted the experiments on the GaN islands, for example, the specific GaN island circled in Fig. 4.4.3. Its height and the diameter are about 9nm and 250nm, respectively. The value of F_{ω} used here represents the averaged ω-force value over the 70nm×70nm area of the island on the ω-force mapping (Fig. 4.4.3 (b)). The value of $F_{tip-p,\omega}$ represents the averaged ω-force value over the 0.2μm×0.2μm region measured at a distance of ~1μm away from islands in Fig. 4.4.3 (b), assuming that the value of $F_{tip-p,\omega}$ does not change no matter at region with or without GaN islands. Since the obtained value of $F_{tip-p,\omega}$ is measured at a featureless plane area away from islands, where exhibits uniform

charge distribution on surface, as shown in Fig. 4.5.2 (c), which is different from the area region around the island, where we assume no ESC in the interface between AlGaN epilayer and the GaN island, as shown in Fig. 4.5.2 (a). Using charge superposition principle, the charge distribution on the island and surrounding area (Fig. 4.5.2 (a)) can be resembled by the equivalent charge distribution described as follows. In equivalent charge distribution, we assume there exhibits charge distributed on the AlGaN under the GaN/AlGaN interface with exactly the same charge density as that of plane area. In order to balance the charge above, we also assume the same interface charge density, however, with opposite polarity, also exists on the GaN island side (signed as solid circles), as shown in Fig. 4.5.2 (d). Consequently, by this arrangement we can subtract the force $F_{tip\text{-}p,\omega}$ resulted from the uniform charge distribution signed as the open circles in Fig. 4.5.2 (c) from F_{ω} by using Eq. (4-7) to obtain the value of the ω-term Coulombic force $F_{is,ESC\text{-}tip,\omega}$ due to the interaction of charges between tip and the specific island, as shown in Fig. 4.5.2 (b). From Fig. 4.5.2 (d), we learn that $F_{is,ESC\text{-}tip,\omega}$ is not due to the surface charge (signed as "**x**") of the island itself, instead, it represents ω-term Coulombic force due to the net surface charge effect owing to the surface charge of island (signed as "**x**") and imaginary interface charge (signed as solid circles) on the island side because the thickness of island (~10nm) is relatively thin as compared with the distance between tip and sample (100~500nm).

Figure 4.5.3 shows the ω-force and 2ω-force intensities vs. tip-sample

distance, which the forces consist of the interactions between tip and both the specific island as well as the plane area around the specific island. Fig. 4.5.4 shows the ω-force and 2ω-force intensities vs. tip-sample distance, which the forces are both between the tip and the plane around the specific island. By referring Eq. (4-7), we can deduce the ω-term Coulombic force intensity vs. tip-sample distance, which the force is between the tip and the surface ESC on the specific GaN island, as shown in Fig. 4.5.5.

Figure 4.5.6 shows the fitting result of the data in Fig. 4.5.4 (a) by cone model, which represents that the tip-sample distance dependence of the ω-force can be interpreted by cone model. The fitting parameters L, R, and θ are 14μm, 11nm, and 12°, respectively. We would use those parameters to fit the following data.

In our fittings, we viewed the single GaN island as a thin disk because of its disk-like shape and the height of the island being much smaller than the tip to sample distance. And in the range of the tip to sample distance in our experiments, the charge distribution of the tip was viewed as uniformly charged line, point charge, and cone, respectively, which were proposed in the published literature. [40-41] Therefore, we used uniformly charged line-disk model, charged point-disk model, and cone model to fit the data in Fig. 4.5.5, respectively. The calculation of the models is discussed as follows.

(I) Uniformly charged line-disk model

Figure 4.5.7 shows the schematic of uniformly charged line-disk model.

The force between uniformly charged line and the uniform ESC density on the GaN island whose radius is 125nm as mentioned above. We use a well-known example in the textbook about electromagnetics to calculate the force between the uniformly charged line and the disk, as shown in Fig. 4.5.7. The formula [42] for the electric field of the well-known example is

$$\vec{E} = \hat{z}\frac{\rho_s}{2\varepsilon_0}\left[1 - z(z^2 + b^2)^{-0.5}\right] \tag{4-8}$$

The schematic diagram is shown in Fig. 4.5.8. The ρ_s in Eq. (4-8) is the charge density of the disk in Fig. 4.5.8. In Fig. 4.5.7, when integrating the Eq. (4-8) with respect to the charged line length element dZ', we can obtain the total electrostatic force F

$$F = \lambda\frac{\rho_s}{2\varepsilon_0}\int\left\{1 - (Z + Z')\left[(Z' + Z)^2 + b^2\right]^{-0.5}\right\}dZ' \tag{4-9}$$

According to the report of S. Belaidi *et al.* [40], they analyzed the electrostatic forces acting on the tip in AFM and the result is in Table 1 [40]. It is noted that the results in Table 1 are in the assumption of infinite plane. And the $\lambda(\theta)$ is obtained as follows when an infinite cone with a half angle θ [40]:

$$\lambda = \frac{2\pi\varepsilon_0 V_0}{\mathrm{Argsh}(\tan^{-1}\theta)}$$

(II) Charged point-disk model

The schematic diagram is shown in Fig. 4.5.9. If we take point discharge into account and ignore the interaction between side wall of the tip and the single disk-like GaN island, the interaction between the sphere on the pointed

end of the tip and the island is the main contribution of the force. [43-44] We took the sphere as a point-charge located in the center because of the smaller size (~20nm in diameter) relative to the diameter of the disk-like island (~250nm) and convenience. By Eq. (4-8), this model is easily calculated as

$$F = \frac{Q\rho_s}{2\varepsilon_0}\left[1-(Z+R)[(Z+R)^2+b^2)^{-0.5}\right] \tag{4-10}$$

where Q is the point-charge on the pointed end of the tip.

(III) Cone model

Eq.(4-6) in section 4.3 has represented the result.

The fitted results of those models for Fig. 4.5.5 are shown in Fig. 4.5.10. We found that the charged point-disk model is the better model to interpret the interaction between the tip and the surface ESC on the specific GaN island, which is different from the model of the interaction between the tip and the infinite Si wafer resulted from the section 4.3.

Above the infinitely charged plane, the electric field is uniform. Thus, the electric field from the sample surface acts on all part of the tip above the plane. In the experiment on Si wafer, the dimension of Si wafer is so large that the Si wafer is infinite compared with the tip. In this condition, we must take all part of the tip into account when computing the ω-term Coulombic force acting on the tip. Therefore, we must use the cone mode to interpret the ω-term Coulombic force between the tip and the surface ESC on the Si wafer. In addition, in the

single disk-like GaN island whose dimension is finite compared with the tip, the electric field is not uniform and decreases rapidly with increasing height (see Appendix.). So, the more the position approaches to the sample and the more the quantity of charge is, the more the electrical force is. On the probe, the sphere on the pointed end of the tip is the most close to the island and more induced charge assembles there (phenomenon of point discharge). The ω-term Coulombic force acting on the sphere of the tip from the surface ESC on the single disk-like GaN island is the main origin. As a result, we used the charged point-disk model to interpret the force $F_{is,ESC\text{-}tip,\omega}(Z)$.

Table 1. Analytic expressions for the electrostatic force. R is the radius of the tip. Z is the tip to sample distance. L is the length of the tip. θ is half angle of the cone. $s(\theta)=a\theta+b$, $a=0.13$ and $b=0.72$ can be used in the $5<\theta<50$. [40]

	Very small tip-sample distance $Z<R$	Intermediate distance $(R<Z<L)$	Large tip-sample distance $Z>L$
Model	Sphere	Uniformly charged line	Modified sphere
Expression of the force F	$\pi\varepsilon_0 V_0^2 \frac{R}{Z}$	$\frac{\lambda(\theta)^2}{4\pi\varepsilon_0}\ln\left(\frac{L}{4Z}\right)$	$\pi\varepsilon_0 V_0^2\left(\frac{L}{2Z}s(\theta)\right)^2$
Gradient $\frac{\partial F}{\partial Z}$	$\propto \frac{1}{Z^2}$	$\propto \frac{1}{Z}$	$\propto \frac{1}{Z^3}$
Localization of the force on the tip	Apex	Tip side	Not localized

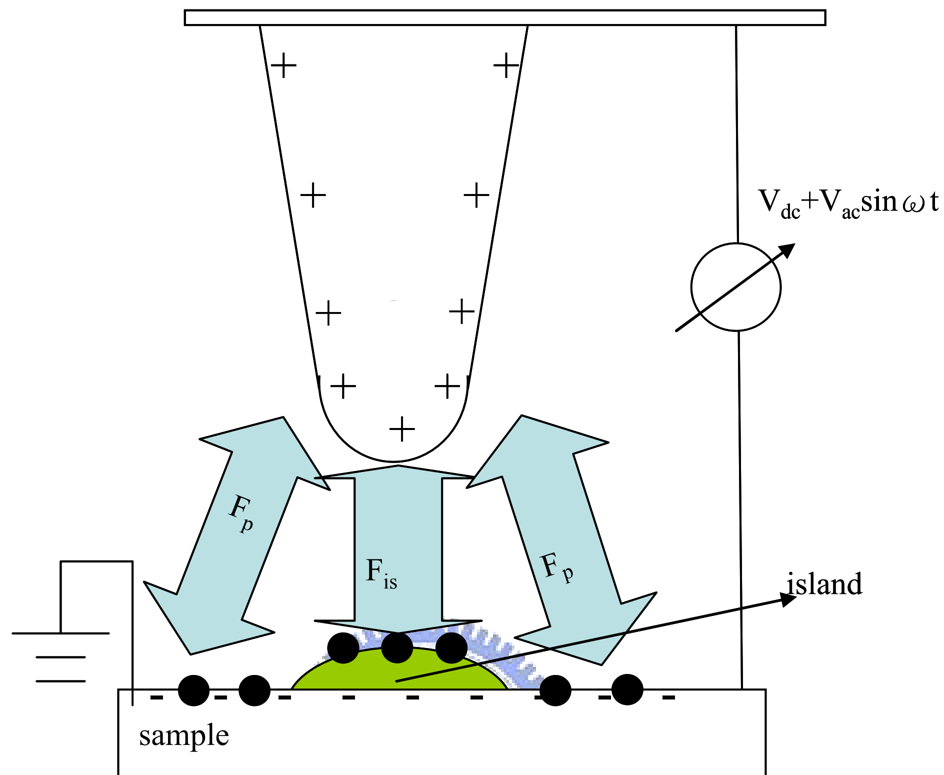

Fig. 4.5.1. Schematic diagram of the interactions between the tip and the sample surface with GaN islands. The "+" and "-" represent the induced charge by biasing, and the solid circles are surface ESC. It is noted that the twin-arrows represent the force. F_{is} is the force between the tip and the specific island. The F_p is the force between the tip and the plane around the specific island. The size of the arrows does not express the intensity of the force.

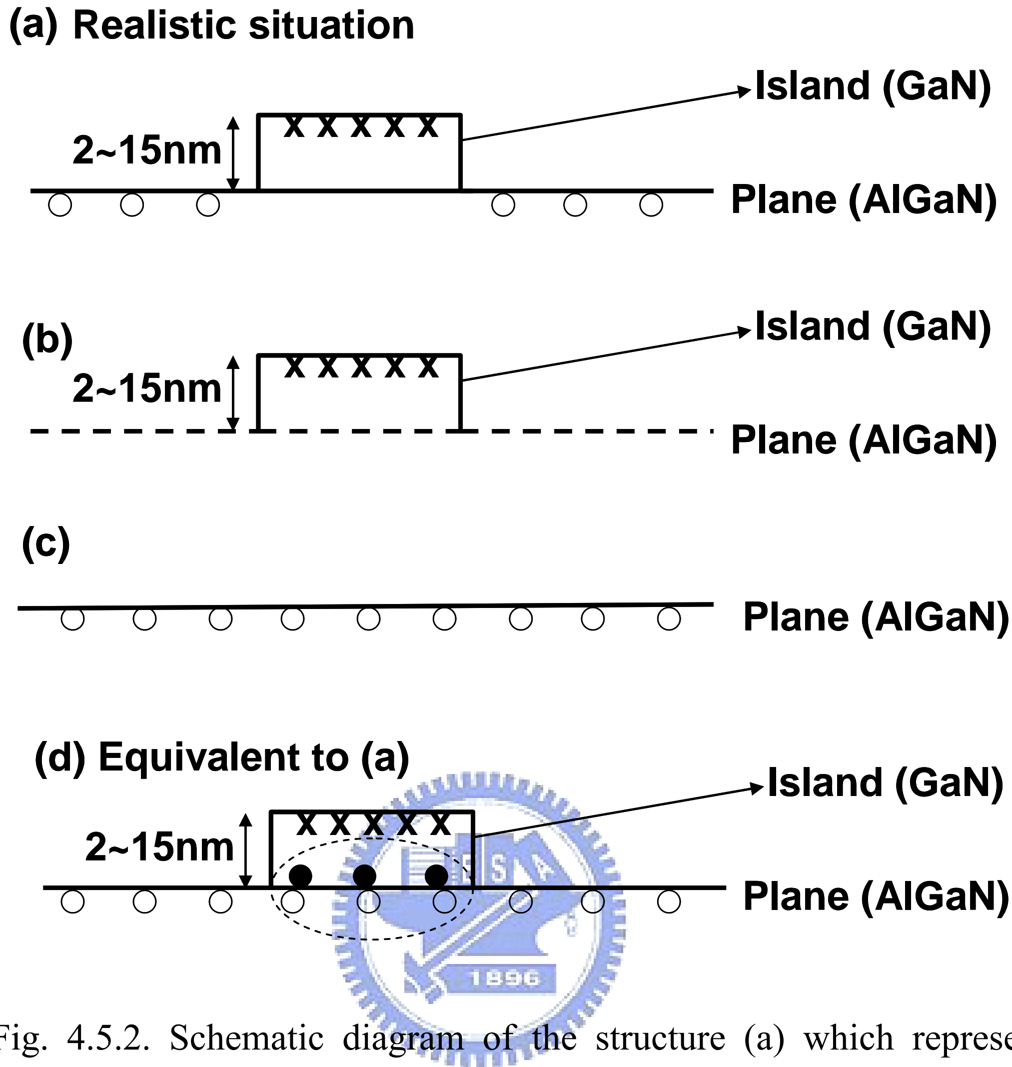

Fig. 4.5.2. Schematic diagram of the structure (a) which represents the realistic distribution of surface ESC on the AlGaN epilayer with GaN island being combined by (b) and (c). (b) and (c) represent the ESC distribution on the GaN island and AlGaN epilayer, respectively. The open circles and "**x**" are expressed as the surface ESC on plane and island, respectively. And the solid circles are expressed as the charge on the lowerside of the GaN island, which is opposite pole to the charge expressed by the open circles. (d) is equivalent to (a) and the circles in the dotted ellipse in (d) express the counter-balanced charge.

(a)

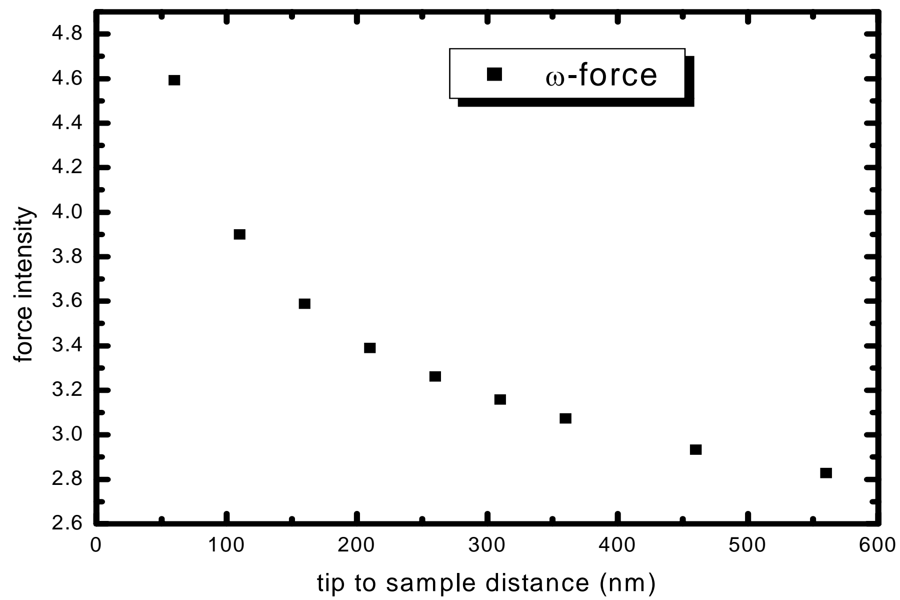

(b)

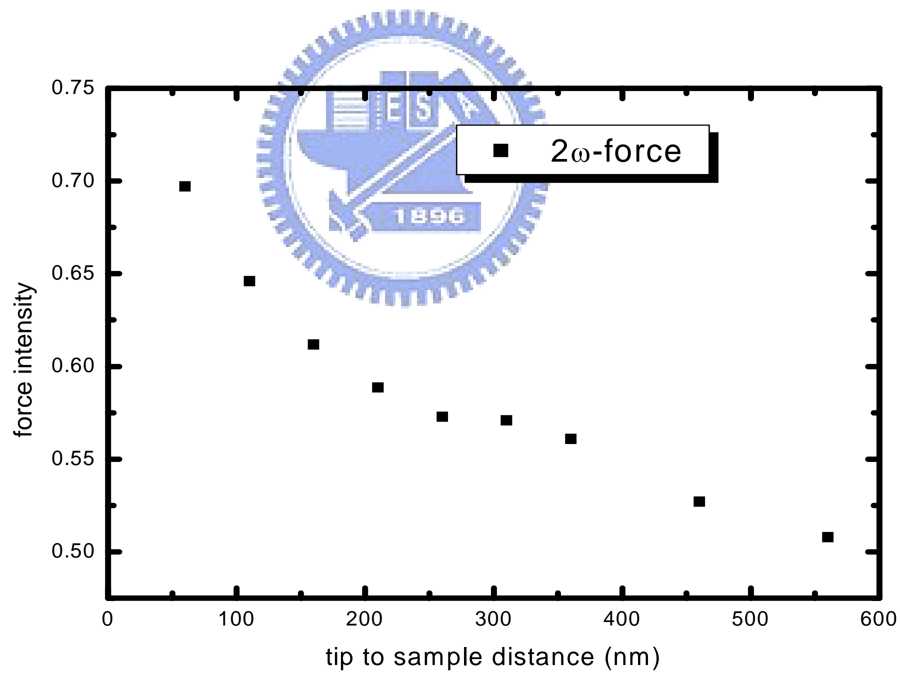

Fig. 4.5.3. The intensities of (a) ω-force and (b) 2ω-force acting on the tip vs. tip-sample distance which the forces consist of F_p and F_{is} indicated in Fig. 4.5.1

.

(a)

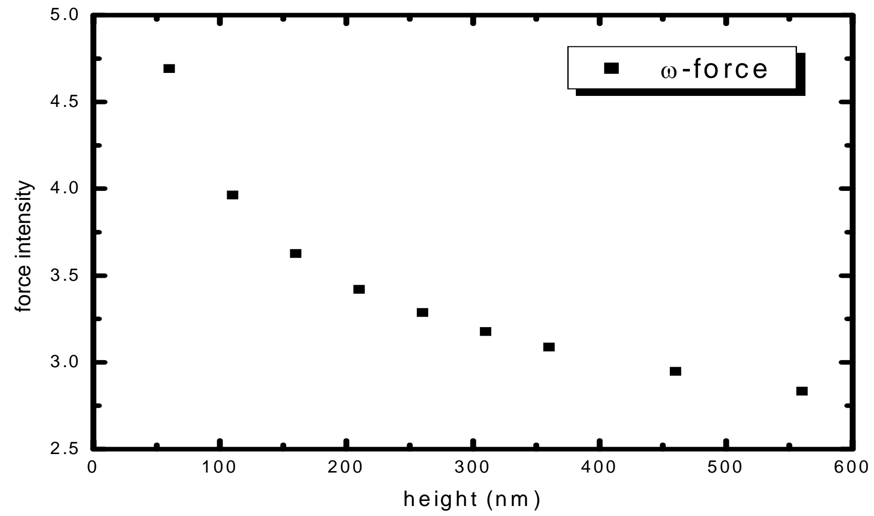

(b)

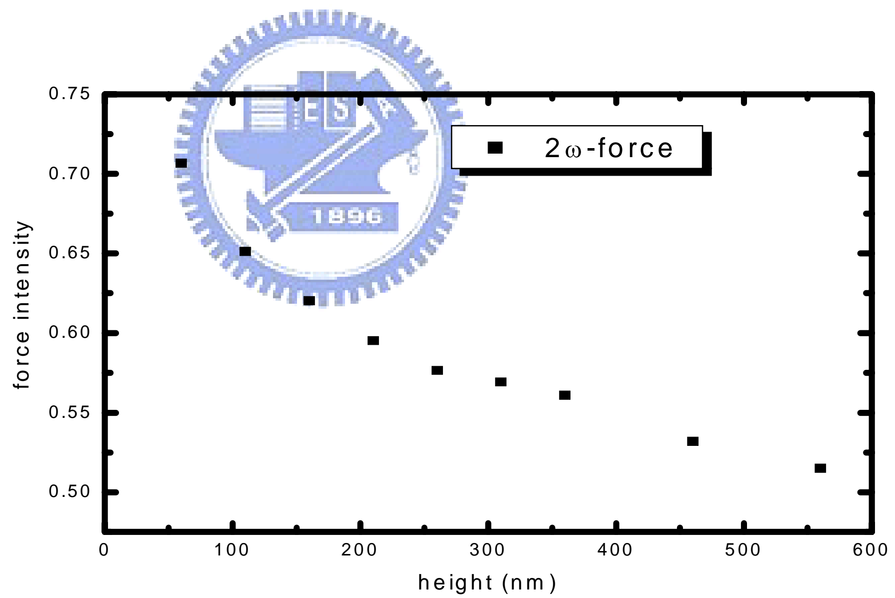

Fig. 4.5.4. The intensities of (a) ω-force and (b) 2ω-force acting on the tip vs. tip-sample distance which the forces are between the tip and the plane around the island.

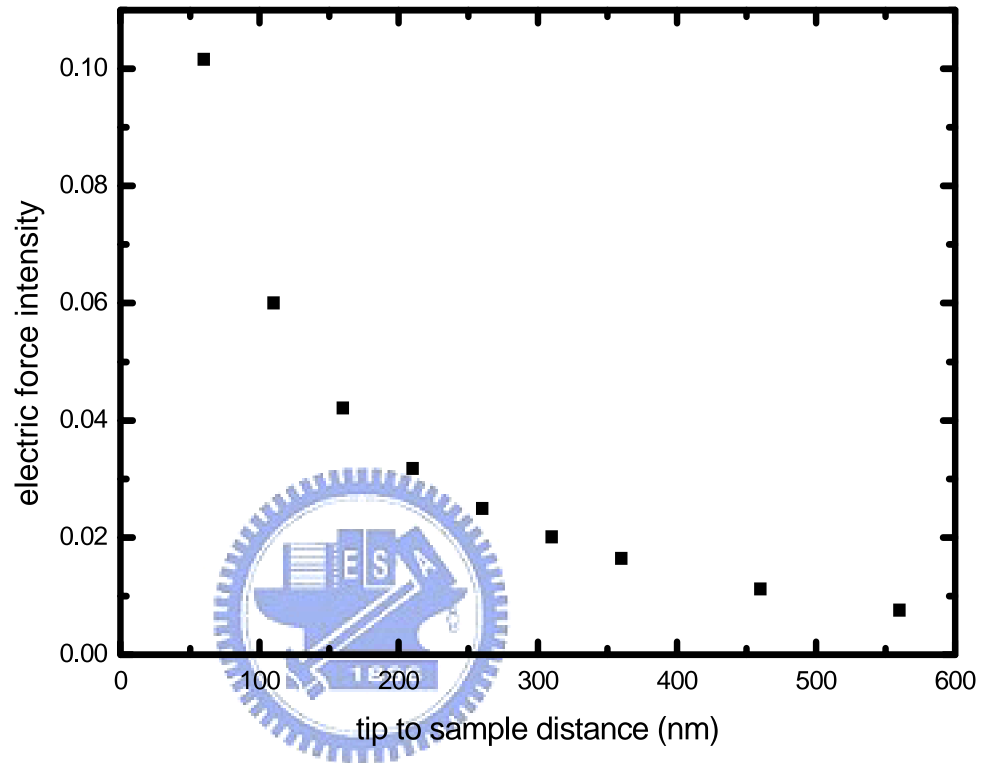

Fig. 4.5.5. The calculated ω-term Coulombic force intensity between the tip and the surface ESC on the specific island vs. tip-sample distance.

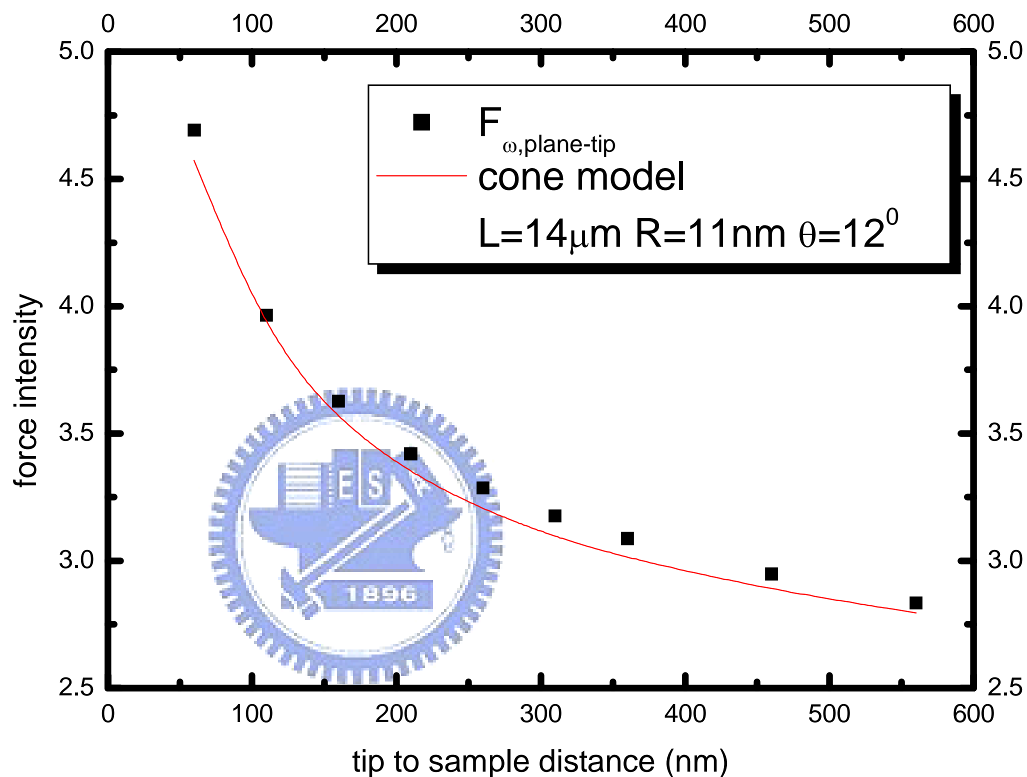

Fig. 4.5.6. The ω-force intensity acting on the tip vs. tip-sample distance on the plane region of the sample and their fitting result by the cone model.

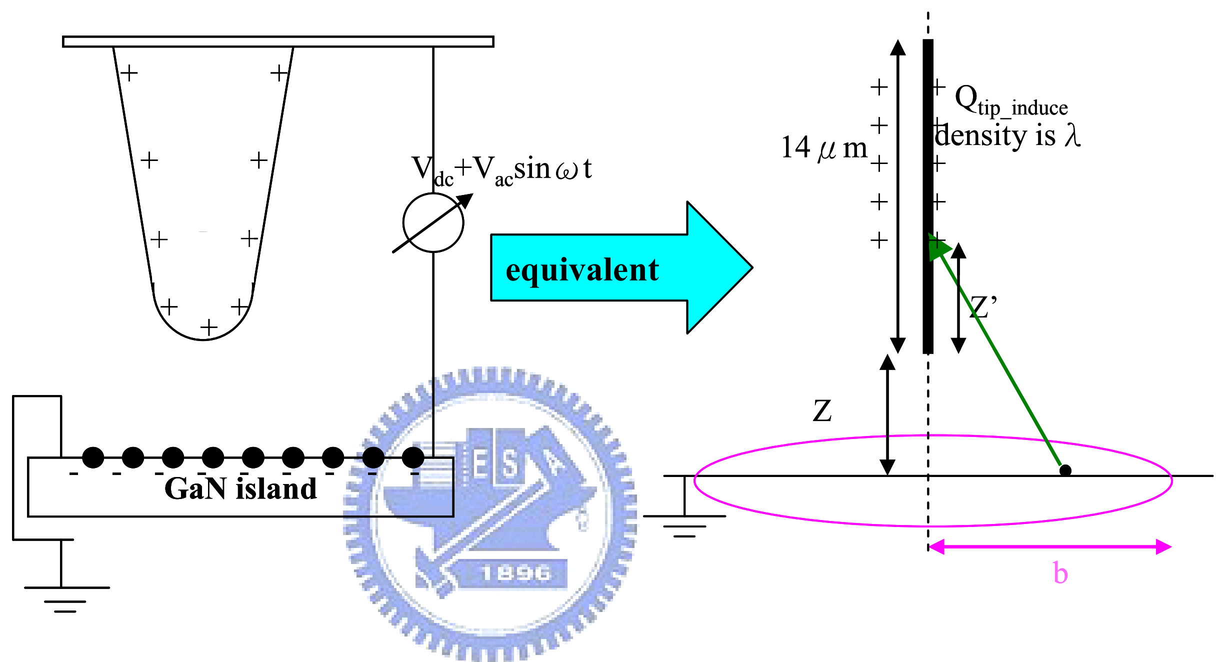

Fig. 4.5.7. Schematic of uniformly charged line-disk model. The “+” and “-“ represent the induced charge by biasing, and the solid circles are surface ESC whose uniform charge density is ρ_s in our assumption.

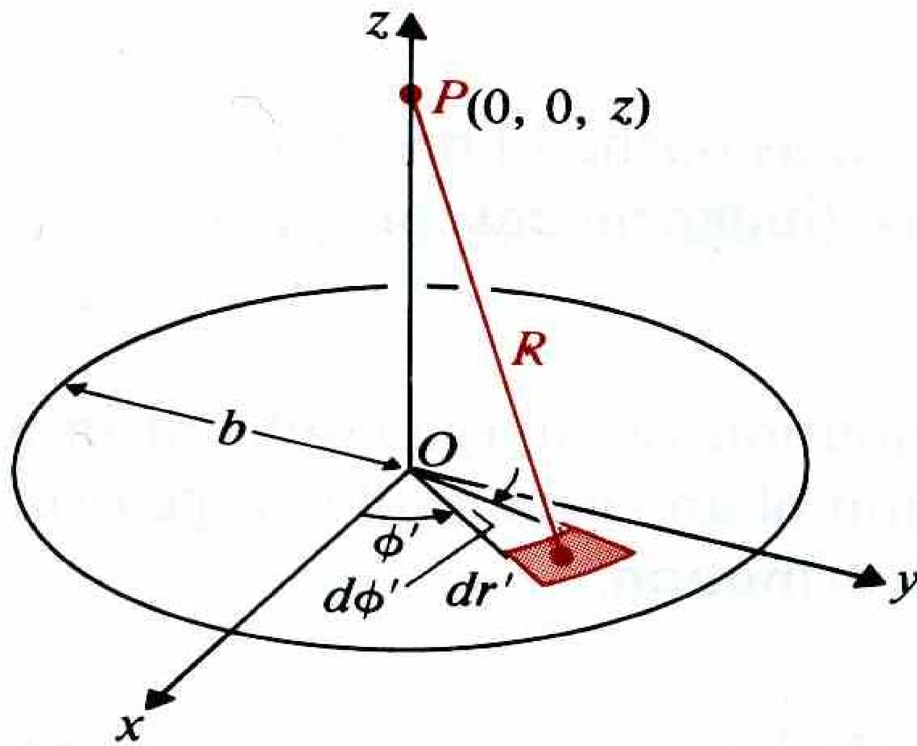

Fig. 4.5.8. Schematic diagram of Eq. (4-8). [42]

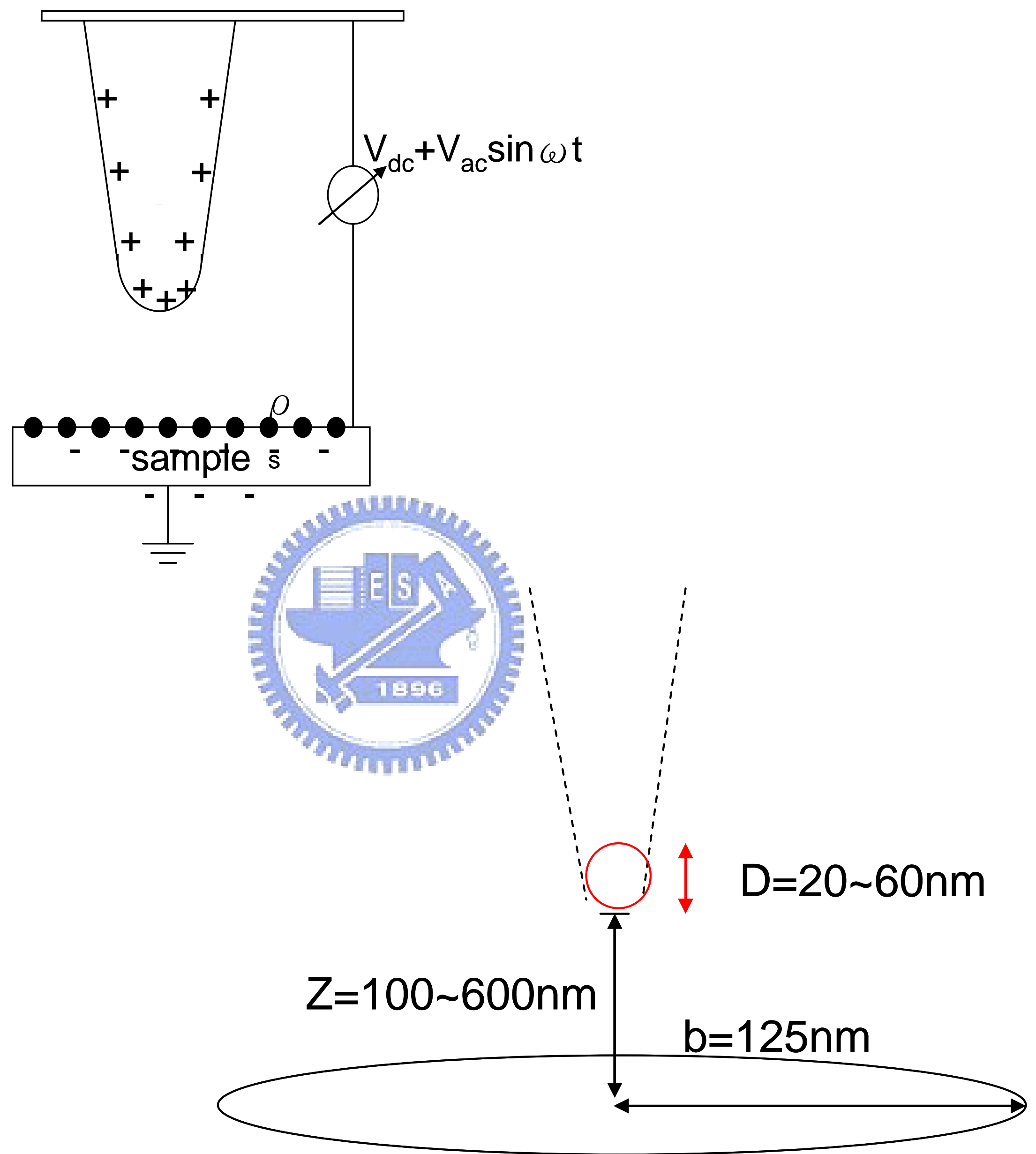

Fig. 4.5.9. Schematic of charged point-disk model.

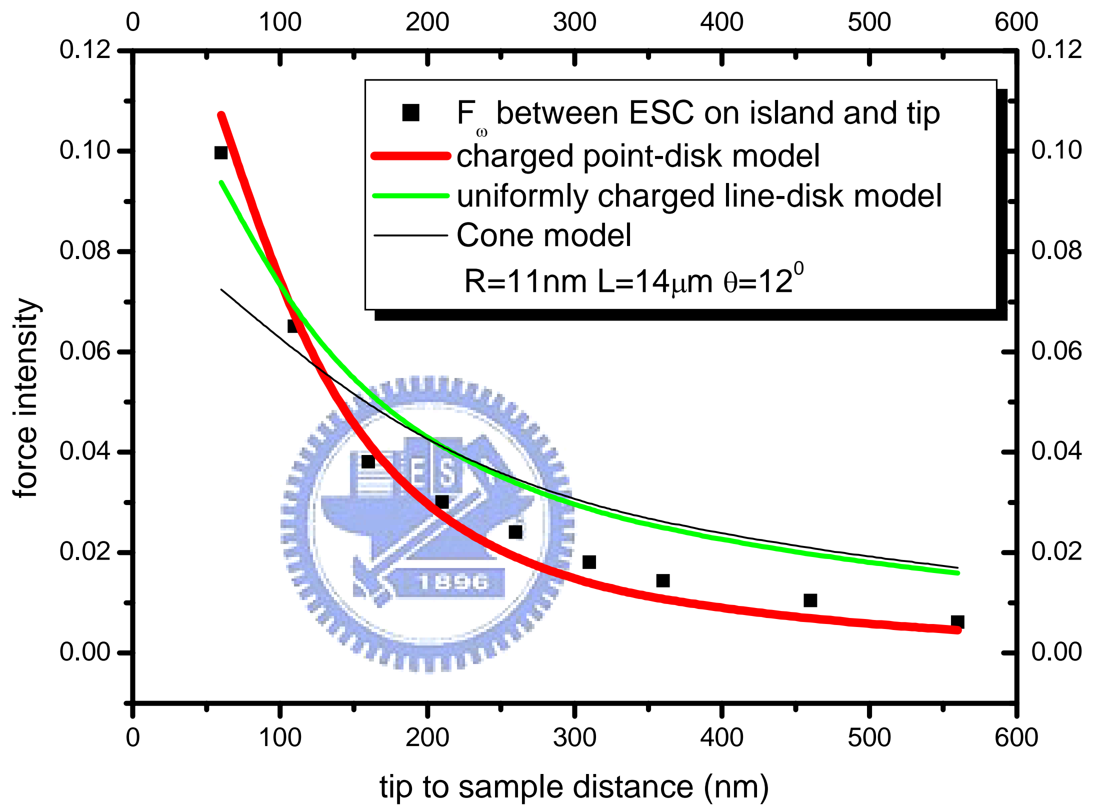

Fig. 4.5.10. The ω-term $F_{is,ESC\text{-}tip}(Z)$ experimental data and the three model fitted results.

Chapter 5 Conclusion

In this thesis, we have developed a model to elucidate the ω-term Coulombic force $F_{ESC-tip,\omega}$ between the tip and the surface ESC on the Si wafer and on the disk-like GaN island, respectively. By the method, we can obtain the surface work function of the tip we used here, which can in turn retrieve the surface work function of other samples using the same tip.

In the scanning EFM experiments, the results show that the ω-term and 2ω-term force mappings on disk-like GaN islands are well-resolved as AFM image. The intensities of electric force F_{ω} and $F_{2\omega}$ on the region of GaN islands were observed appearing to be lower as compared with that at the plane surface. The higher the island is, the stronger the effect is.

According to the model we developed, we also calculated the $F_{ESC-tip,\omega}$ on the sample at different tip-sample distances. We found that for uniform Si wafer the ω-term Coulombic force between tip and surface ESC, $F_{ESC-tip,\omega}(Z)$, can be interpreted by cone model. Furthermore we also carried out scanning EFM for disk-like GaN islands with diameters ranged from ~200 to ~500nm grown on AlGaN epilayer. Our results showed that the ω-term Coulombic force between tip and surface charge $F_{ESC-tip,\omega}(Z)$ for the single GaN island can be interpreted well by the charged point-disk model.

Whenever charged point-disk model or cone model is used to explain for

ω-term Coulombic force between tip and sample depends on radius of tip and diameter of sample. For uniform Si wafer, the dimension can be considered to be infinite compared with the radius of the tip. In this situation, cone mode can be employed to interpret the experimental results because of the infinite Si plane relative to the tip radius and the uniform electric field intensity from the ESC on the Si wafer, which cause the all part of the cone-like tip to be suffered from the electric force from the ESC on the Si wafer. For the single disk-like GaN island whose diameter of disk possesses a finite value as compared with that of the tip, the electric field is not uniform and decreases rapidly with increasing height. On the probe, because the sphere on the pointed end of the tip is the most close to the island and more charge assembles there. That is the part of sphere is the main position suffered the force $F_{is,ESC\text{-}tip}$. As a result, we must use the charged point-disk model to interpret the $F_{is,ESC\text{-}tip}(Z)$ in the case of the single disk-like GaN island.

Appendix

We drew the calculated electric field intensity vs. height (by the Eq. 4-8) in the Fig. A.1 (marked as the black dots). The radius b is replaced with 125nm and the height Z varied from 50nm to 600nm in the calculation, which corresponds to the case of our experiments mentioned in the section 4.5. The fitted results show that the force decays rapidly and the electric field intensity can be ignored when height is larger than about 300nm.

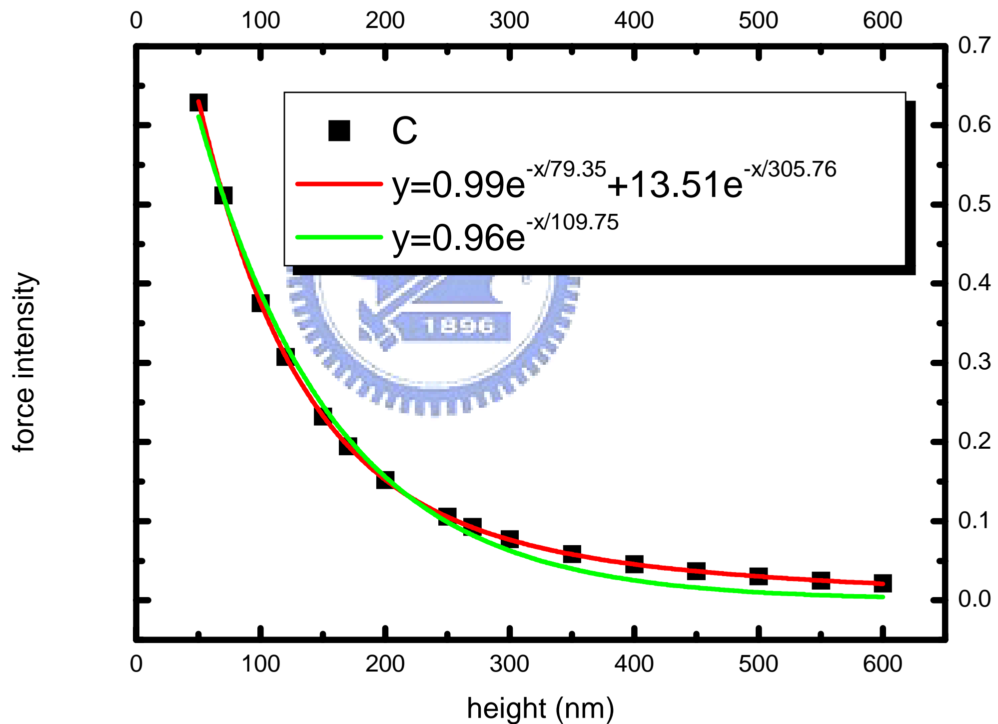

A.1. The electric field intensity vs. height calculated by Eq. (4-8).

Reference：

[1]P. Girard, P. Cadet, M. Ramonda, N. Shmidt, A. N. Usikov, W. V. Lundin, M. S. Dunaevskii, and A. N. Titkov, *Phys. Stat. Sol. (a)* **195**, 508 (2003).

[2]F. Muller, A. D. Muller, M. Hietschold, and S. Kammer, *Meas. Sci. Technol.* **9**, 734 (1998).

[3]K. Wapner, B. Schoenberger, M. Stratmann, and G. Grundmeier, *J. Electrochem. Soc.* **152**, E114 (2005).

[4]T. Yamauchi, M. Tabuchi, and A. Nakamura, *Appl. Phys. Lett.* **84**, 3834 (2004).

[5]A. Efimov, and S. R. Cohen, *J. Vac. Sci. Technol. A* **18**, 1051 (2000).

[6]G. Koley and M. G. Spencer, *Appl. Phys. Lett.* **78**, 2873 (2001).

[7]T. Mizutani, T. Usunami, S. Kishimoto and K. Maezawa, *Jpn. J. Appl. Phys.* **38**, L767 (1999).

[8]T. Takahashi, T. Kawamukai, S. Ono, T. Noda, and H. Sakaki, *Jpn. J. Appl. Phys.* **39**, 3721 (2000).

[9]S. Ono, M. Takeuchi, and T. Takahashi, *Appl. Phys. Lett.* **78**, 1086 (2001).

[10]Y. Eguchi, S. Kishimoto, and T. Mizutani, *Jpn. J. Appl. Phys.* **40**, L589 (2001).

[11]S. Ono, M. Takeuchi, T. Noda, and T. Takahashi, *Jpn. J. Appl. Phys.* **42**, 4869 (2003).

[12]B. S. Simpkins, D. M. Schaadt, E. T. Yu, and R. J. Molnar, *J. Appl. Phys.* **91**, 9924 (2002).

[13]J. W. P. Hsu, H. M. Ng, A. M. Sergent, and S. N. G. Chu, *Appl. Phys. Lett.* **81**, 3579 (2002).

[14]Y. Rosenwaks, R. Shikler, T. Glatzel, and S. Sadewasser, *Phys. Rev. B* **70**, 085320 (2004).

[15]J. Jiang, T. D. Krauss, and L. E. Brus, *J. Phys. Chem. B* **104**, 11936 (2000).

[16]B. D. Huey and D. A. Bonnell, *Solid State Ionics* **131**, 51, (2000).

[17]G. Koley and M. G. Spencer, *J. Appl. Phys.* **90**, 337 (2001).

[18]B. D. Terris, J. E. Stern, D. Rugar, and H. J. Mamin, *Phys. Rev. Lett.* **63**, 2669 (1989).

[19]H. Bluhm, A. Wadas, R. Wiesendanger, K.-P. Meyer, and L. Szczesniak, *Phys. Rev. B* **55**, 4 (1997).

[20]R. M. Nyffenegger, R. M. Penner, and R. Schierle, *Appl. Phys. Lett.* **71**, 1878 (1997).

[21]P. M. Bridger, Z. Z. Bandic, E. C. Piquette, and T. C. McGill, *Appl. Phys. Lett.* **74**, 3522 (1999).

[22]J. J. O'Shea, M. D. Camras, D. Wynne, and G. E. Hofler, *J. Appl. Phys.* **90**, 4791 (2001).

[23]See, for example, D. Bonnell, ed., *Scanning probe microscopy and spectroscopy: theory, techniques, and applications, 2nd ed.* Wiley-VCH, New York, 2001.

[24]J. W. Hong, S.-I. Park, and Z. G. Khim, *Rev. Sci. Instrum.* **70**, 1735 (1999).

[25]J. W. Hong, K. H. Noh, S.-I. Park, S. I. Kwun, and Z. G. Khim, *Phys. Rev. B* **58**, 5078 (1998).

[26]F. Saurenbach and B. D. Terris, *Appl. Phys. Lett.* **56**, 1703 (1990).

[27]O. Cherniavskaya, L. Chen, V. Weng, L. Yuditsky, and L. E. Brus, *J. Phys. Chem. B* **107**, 1525 (2003).

[28]T. D. Krauss, S. O'Brien, and L. E. Brus, *J. Phys. Chem. B* **105**, 1725 (2001).

[29]Z.-Y. Wang, J.-B. Bao, H.-H. Zhang, and W.-M. Guo, *Appl. Phys. Lett.* **81**, 1300 (2002).

[30]B. J. Rodriguez, W.-C. Yang, R. J. Nemanich, and A. Gruverman, *Appl. Phys. Lett.* **86**, 112115 (2005).

[31]J. W. Hong, D. S. Kahng, J. C. Shin, H. J. Kim, and Z. G. Khim, *J. Vac. Sci. Technol. B* **16**, 2942 (1998).

[32]G. M. Sacha, and J. J. Saenz, *Appl. Phys. Lett.* **85**, 2610 (2004).

[33]J. Colchero, A. Gil, and A. M. Baro, *Phys. Rev. B* **64**, 245403 (2001).

[34]G. Koley, M. G. Spencer, and H. R. Bhangale, *Appl. Phys. Lett.* **79**, 545 (2001).

[35]P. Girard, A. N. Titkov, M. Ramonda, V. P. Evtikhiev, and V. P. Ulin, *Appl. Surf. Sci.* **201**, 1 (2002).

[36]P. Girard, *Nanotechnology* **12**, 485 (2001).

[37]The work function of i-Si is calculated from the equation $\Phi_{i-Si} = \chi_{Si} - \frac{1}{2}E_{g,\,Si}$ where Φ, χ, and E_g represent the work function, electron affinity and bandgap energy, respectively. The latter two values are 4.01eV and 1.12eV, respectively. (refered to the Table B.4 in Ref. 38) So, we adopted 4.6eV as the work function of i-Si, which is figure out by the equation above.

[38]D. A. Neamen, *Semiconductor physics and devices: basic principles, 3rd ed.*, p.328, McGraw-Hill, New York, 2003.

[39]S. Patil, A. V. Kulkarni, and C. V. Dharmadhikari, *J. Appl. Phys.* **88**, 6940 (2000).

[40]S. Belaidi, P. Girard, and G. Leveque, *J. Appl. Phys.* **81**, 1023 (1997).

[41]H. W. Hao, A. M. Baro, and J. J. Saenz, *J. Vac. Sci. Technol. B* **9**, 1323 (1991).

[42]See, for example, D. K. Cheng, *Field and wave electromagnetics, 2nd ed.*, p.98-99, Addison-Wesley, Reading Massachusetts, 1992.

[43]G. M. Sacha, A. Verdaguer, J. Martinez, J. J. Saenz, D. F. Ogletree, and M. Salmeron, *Appl. Phys. Lett.* **86**, 123101 (2005).

[44]S. Watanabe, K. Hane, T. Ohye, M. Ito, and T. Goto, *J. Vac. Sci. Technol. B* **11**, 1774 (1993).